AFOSR URI

HIGH TEMPERATURE COMPOSITES: PROPERTIES, PROCESSING AND PERFORMANCE

FINAL REPORT

MAY 16, 1993 - MAY 15, 1998

UNIVERSITY OF VIRGINIA

PROJECT DIRECTOR: CARL T. HERAKOVICH

FACULTY:

JACOB ABOUDI
SARAH C. BAXTER
DANA M. ELZEY
CARL T. HERAKOVICH
ROLAND H. KRAUSS
GABRIEL LAUFER
MAREK-JERZY PINDERA
HAYDN N. G. WADLEY
FRANKLIN E. WAWNER, JR.

AFOSR #F49620-93-1-0359

SCHOOL OF
ENGINEERING
& APPLIED SCIENCE

University of Virginia
Thornton Hall
Charlottesville, VA 22903

UNIVERSITY OF VIRGINIA
School of Engineering and Applied Science

The University of Virginia's School of Engineering and Applied Science has an undergraduate enrollment of approximately 1,500 students with a graduate enrollment of approximately 600. There are 160 faculty members, a majority of whom conduct research in addition to teaching.

Research is a vital part of the educational program and interests parallel academic specialties. These range from the classical engineering disciplines of Chemical, Civil, Electrical, and Mechanical and Aerospace to newer, more specialized fields of Applied Mechanics, Biomedical Engineering, Systems Engineering, Materials Science, Nuclear Engineering and Engineering Physics, Applied Mathematics and Computer Science. Within these disciplines there are well equipped laboratories for conducting highly specialized research. All departments offer the doctorate; Biomedical and Materials Science grant only graduate degrees. In addition, courses in the humanities are offered within the School.

The University of Virginia (which includes approximately 2,000 faculty and a total of full-time student enrollment of about 17,000), also offers professional degrees under the schools of Architecture, Law, Medicine, Nursing, Commerce, Business Administration, and Education. In addition, the College of Arts and Sciences houses departments of Mathematics, Phyics, Chemistry and others relevant to the engineering research program. The School of Engineering and Applied Science is an integral part of this University community which provides opportunities for interdisciplinary work in pursuit of the basic goals of education, research, and public service.

REPORT DOCUMENTATION PAGE

Form Approved
OMB No. 0704-0188

1. AGENCY USE ONLY *(Leave blank)*	2. REPORT DATE	3. REPORT TYPE AND DATES COVERED
	May 21, 1998	Final Technical Report 15 May 93 to 14 May 98

4. TITLE AND SUBTITLE
High Temperature Composites: Properties, Processing and Performance

5. FUNDING NUMBERS
F49620-93-1-0359

6. AUTHOR(S)
Carl T. Herakovich

7. PERFORMING ORGANIZATION NAME(S) AND ADDRESS(ES)
University of Virginia
B122 Thornton Hall, Applied Mechanics Program
School of Engineering & Applied Science
Charlottesville, VA 22903-2442

8. PERFORMING ORGANIZATION REPORT NUMBER

9. SPONSORING/MONITORING AGENCY NAME(S) AND ADDRESS(ES)
AFOSR/NA
110 Duncan Avenue, Suite B115
Bolling AFB, DC 20332-8050

10. SPONSORING/MONITORING AGENCY REPORT NUMBER
F49620-93-1-0359

11. SUPPLEMENTARY NOTES

12a. DISTRIBUTION AVAILABILITY STATEMENT
Approved for Public Release; Distribution Unlimited.

12b. DISTRIBUTION CODE

13. ABSTRACT *(Maximum 200 words)*
The results of the five year grant (including one year of no-cost extension) are reported. The main accomplishments of the grant activity were fabrication, modelling and testing of a hybrid ceramic fiber and nickely alloy matrix composites suitable for higher temperature applications at lower cost.

14. SUBJECT TERMS

15. NUMBER OF PAGES

16. PRICE CODE

17. SECURITY CLASSIFICATION OF REPORT	18. SECURITY CLASSIFICATION OF THIS PAGE	19. SECURITY CLASSIFICATION OF ABSTRACT	20. LIMITATION OF ABSTRACT
Unclassified	Unclassified	Unclassified	UL

AFOSR URI

HIGH TEMPERATURE COMPOSITES: PROPERTIES, PROCESSING AND PERFORMANCE

FINAL REPORT:

MAY 16, 1993 - MAY 15, 1998

UNIVERSITY OF VIRGINIA

PROJECT DIRECTOR: CARL T. HERAKOVICH

FACULTY:

JACOB ABOUDI
SARAH C. BAXTER
DANA M. ELZEY
CARL T. HERAKOVICH
ROLAND H. KRAUSS
GABRIEL LAUFER
MAREK-JERZY PINDERA
HAYDN N. G. WADLEY
FRANKLIN E. WAWNER, JR.

AFOSR #F49620-93-1-0359

Grant Monitors: Dr. Walter F. Jones, Major Brian Sanders, Dr. Ozden Ochoa

TABLE OF CONTENTS

Center for High Temperature Composites

Our Primary Goal:

To extend the operating temperatures of metal matrix composites

Matrix and Fiber Selection

(Oxidation Stability)

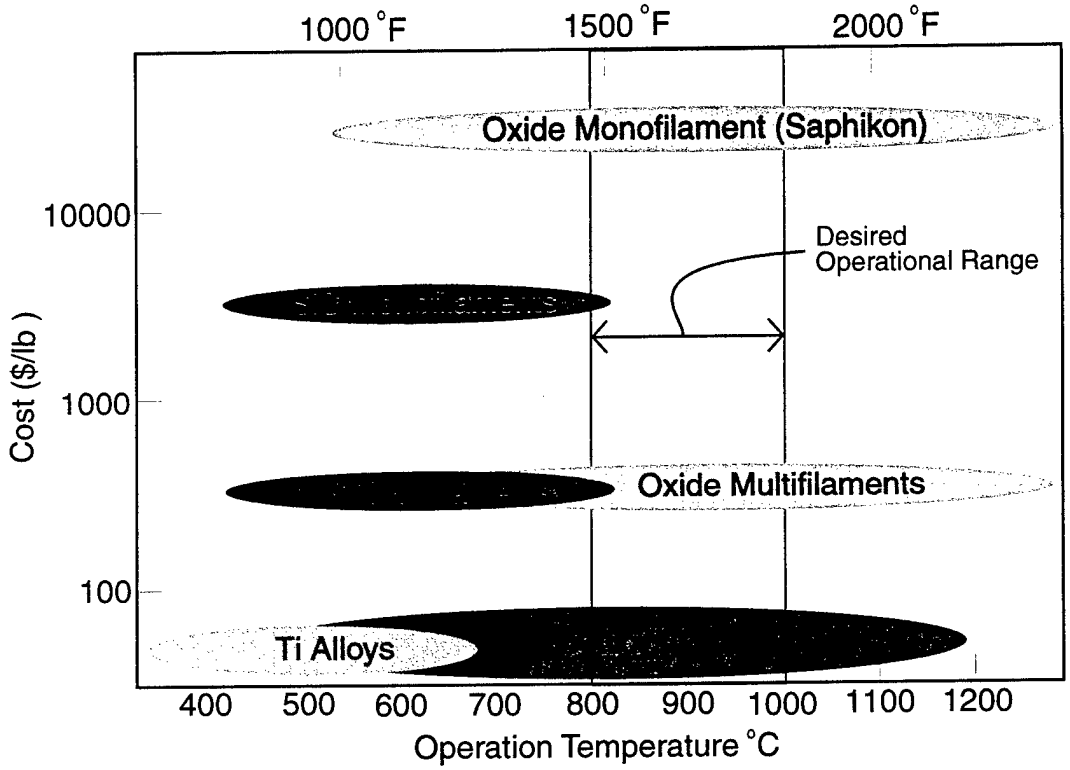

Specific Strength versus Testing Temperature

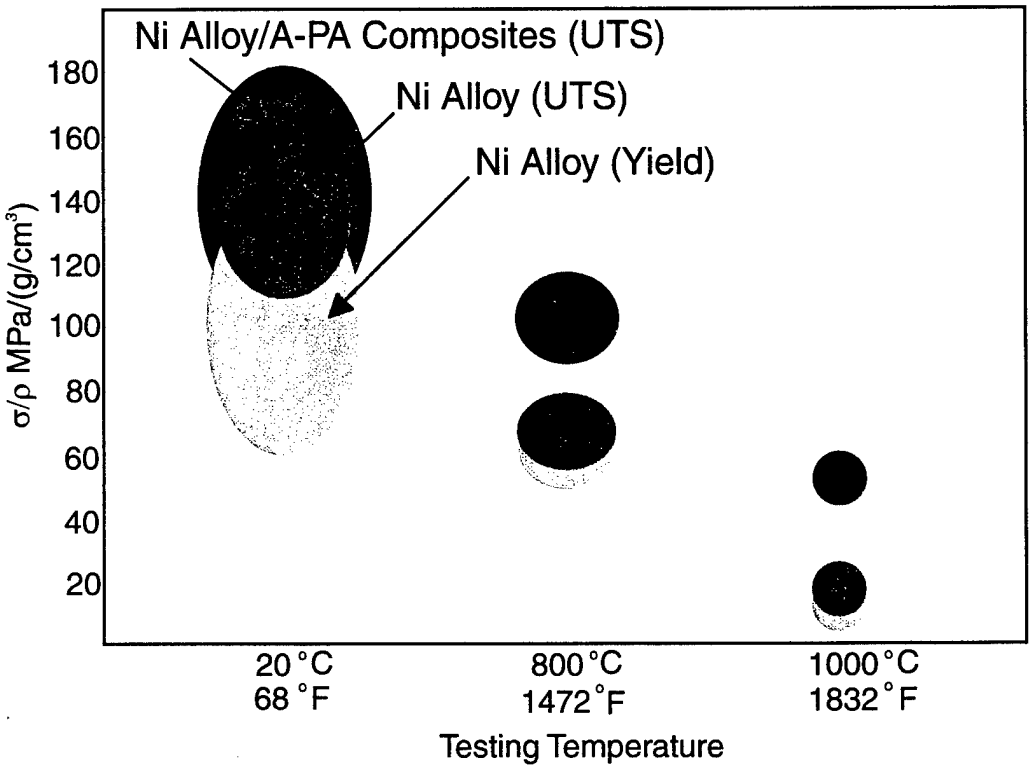

Stress for creep extension of 0.1% in 300 hr. versus Testing Temperature

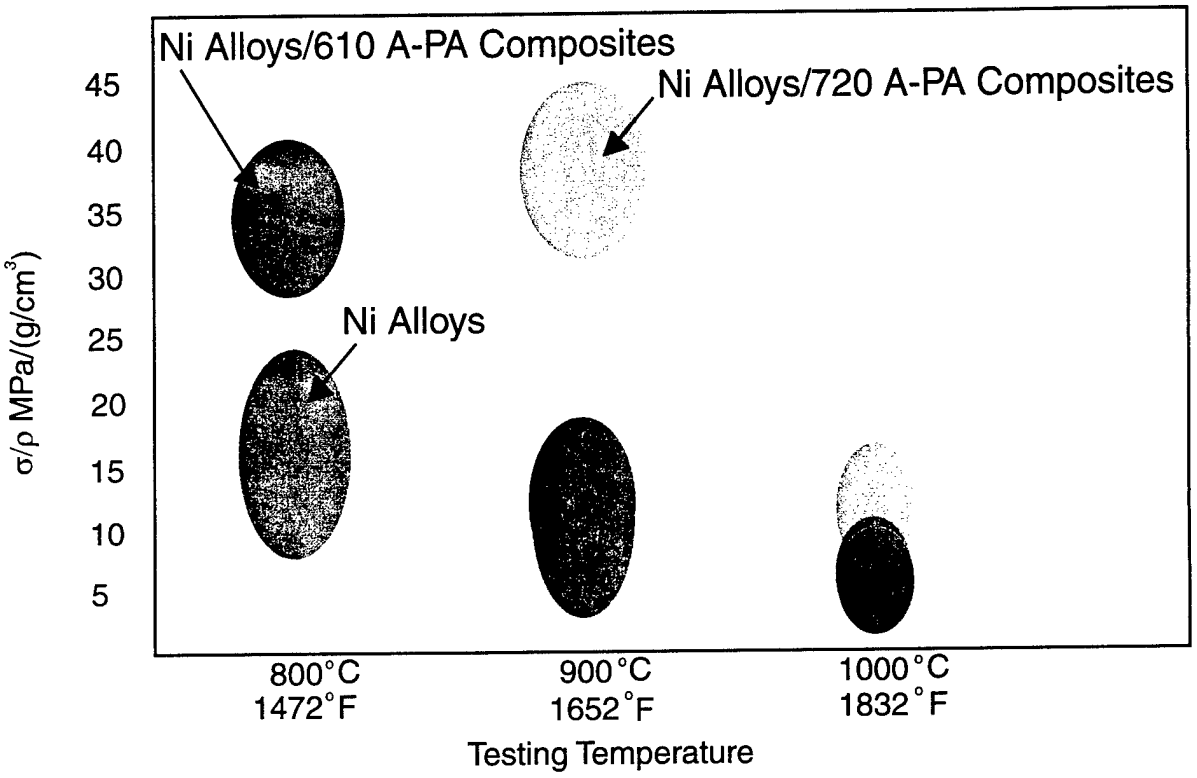

Biomimetic Hybrid Fiber Approach

Non-Uniform Filament Distribution

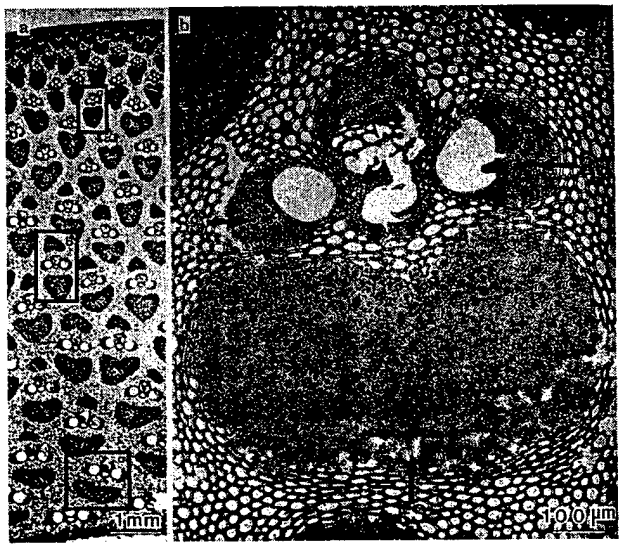

Bamboo

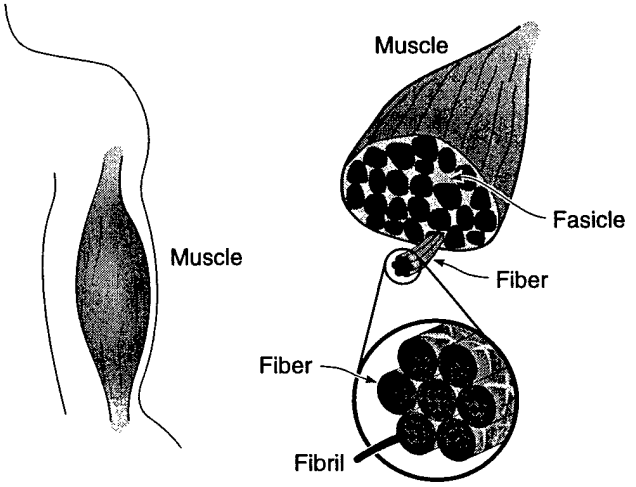

Muscle Tissue

TMC

COMPOSITE CONSTITUENTS

A-PA HYBRID FIBER

- ALUMINA (NEXTEL 610, AL_2O_3) FIBERS IN POROUS ALUMINA BINDER

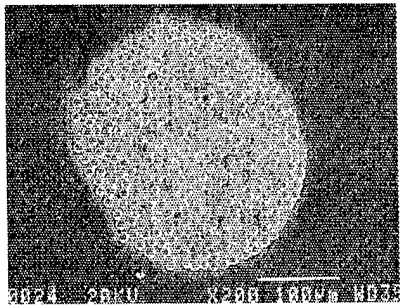

A-PA HYBRID FIBER

MATRIX

- IC50 NICKEL ALUMINIDE
- HAYNES 230 NICKEL SUPERALLOY (NICKEL-CHROMIUM-TUNGSTEN)

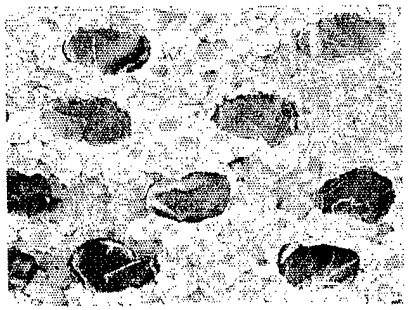

A-PA/MMC

MAJOR ACCOMPLISHMENTS

FABRICATION:

- SUCCESSFULLY PROCESSED A-PA HYBRID FIBERS CONSISTING OF NEXTEL 610 ALUMINA (AL_2O_3) FILAMENTS IN A POROUS ALUMINA BINDER.
- SUCCESSFULLY MANUFACTURED A-PA HYBRID FIBER REINFORCED NI-ALLOY METAL MATRIX (IC50 & HAYNES 230) COMPOSITES VIA TAPE CASTING.

MODELING:

- FOUND THAT THE IDEAL BUNDLE MODEL PREDICTS THE STRESS/STRAIN RESPONSE OF AS-RECEIVED AL_20_3 BUNDLES (NEXTEL 610).
- DEVELOPED A MICROMECHANICS-BASED MODEL FOR PREDICTING THE RESIDUAL STATE OF STRESS AND STRAIN IN A-PA/IC50 AS A RESULT OF FABRICATION INCLUDING THE EFFECTS OF THE HIP CAN.
- DEVELOPED A MICROMECHANICS MODEL FOR PREDICTING THE EFFECTS OF PORE GEOMETRY AND PERCENT POROSITY ON THE VISCOPLASTIC RESPONSE OF POROUS MEDIA.
- DEVELOPED A MICROMECHANICS METHODOLOGY FOR STUDYING THE INFLUENCE OF POROSITY AND MATRIX VISCOPLASTICITY ON THE RESPONSE OF POROUS METAL MATRIX COMPOSITES.

MAJOR ACCOMPLISHMENTS

EXPERIMENTAL:

- FOUND NON-IDEAL BEHAVIOR OF AL_2O_3 BUNDLES AT THE HIGHER HEAT TREATMENT TEMPERATURES; ATTRIBUTED THIS TO FILAMENT/FILAMENT SINTERING.
- DETERMINED THAT THE STRENGTH OF THE A-PA FIBER INCREASES WITH INCREASING POROSITY.
- DEMONSTRATED SIGNIFICANTLY HIGHER FAILURE STRAINS FOR HAYNES 230 COMPARED WITH IC50.
- DEMONSTRATED EXCELLENT CORRELATION BETWEEN MICROMECHANICAL PREDICTIONS FOR AXIAL AND TRANSVERSE MODULUS OF A-PA/HAYNES 230.
- SUCCESSFULLY MEASURED THE MECHANICAL RESPONSE OF A-PA/IC50 AT 617°C OBTAINING INDICATIONS OF HIGH PERCENT RETENTION OF MODULUS AT 617°C.
- SHOWED THAT THE ADDITION OF POROUS BINDER TO FIBER BUNDLES DRAMATICALLY ALTERS CREEP RESPONSE.
- OBTAINED EXPERIMENTAL RESULTS FOR THE CTE OF NEAT IC50, A-PA HYBRID FIBER AND A-PA/IC50 MMC OVER THE TEMPERATURE RANGE OF 25°C TO 750°C.

MAJOR ACCOMPLISHMENTS

EXPERIMENTAL:

- DEMONSTRATED BONDING OF Dy+3:YAG THERMOGRAPHIC PHOSPHOR TO NICKEL SUBSTRATES BY DIRECT FUSING AND WITH SPEREX BINDER FOR HEATING UP TO 925°C.
- DEMONSTRATED PLANAR IMAGING OF THE TEMPERATURE DISTRIBUTION ON THE COATED SAMPLE OVER A RANGE OF 25°C - 925°C.
- DEMONSTRATED THE SIMULTANEOUS MEASUREMENT OF STRAIN AND TEMPERATURE.

GRADUATE STUDENTS

Name	Degree	Thesis Title
Cantonwine, Paul E.	Ph.D.	The Effects of High Temperature aging on the Mechanical Response of an Oxide/Oxide Ceramic Matrix Composite
Crow, Phillip D.	Ph.D.	Constitutive Models For Reinforced Porous Power Law Materials
Dunn, Patrick T.	M.S.	Analysis Of An Interfacial Tension Strength Test Specimen For Advanced Composites
Edge, Alison E.	M.S.	Imaging of Temperature and In-Plane Strain Distribution of High Temperature surfaces
Groves, James	Ph.D.	Directed Vapor Deposition
Hammond, Vince H.	Ph.D	Creep Response of Alumina Tows and Hybrid Fibers
Hass, D.D.	Ph.D.	Directed Vapor Deposition
Hersh, Cheryl L.	M.S.	A 2D Cylindrical Finite Element For 3D Analysis of Stiffened Composites
McGarry, Thomas D.	M.S.	Evaluation of Various Metal Oxide Ceramic Diffusion Barrier Coatings For SCS-2 IN Ti-24A1-11NB
Prins, Rob J.	M.S.	Optical Measurements of Surface Temperature and Strain
Roerden, Alysha M.	M.S.	Micromechanical Modeling of the Inelastic, Thermomechanical Response of Hybrid Fiber, Metal Matrix Composites
Russel, D.T.	M.S.	Creep of Titanium Matrix Composite: Models and Mechanisms
Schroedter, Robert D.	M.S.	Mesoscale Damage Modeling of the Laminated Carbon Fiber-Polyimide Matrix Composite IM7/K3B
Sealing, C. Scott	M.S.	Probabilistic Damage Modeling for Bi-Axial Stress States
Westring, Brice D.	M.S.	Simultaneous Measurements of Strain and Temperature Distributions Using Digital Imaging Methods
Williams, Todd	Ph.D.	Inelastic Microstructural Modeling of Metal Matrix Composites
Yu, Shin C. (John)	M.S.	Process-Structure Relationships for Fiber-Reinforced Composites Produced by Slurry Casting

RESEARCH ASSISTANTS: Eman Siragy, Sebastien Le Loch

PUBLICATIONS & PRESENTATIONS

Papers:

- Baxter, S. C. and Pindera, M-J., "Response of MMC Tubes with Internal Fiber Cracks," in Proc. 11th ASCE Engineering Mechanics Conference, Y. K. Lin and T. C. Su (Eds.), pp. 412-415, 1996. ASCE, New York.
- Baxter, S.C. and Pindera, M-J, ``Degradation of elastic response of MMC laminated tubes due to internal fiber crack's", J. Aerospace Engineering, 10:1 pp 43-48, 1997.
- Baxter, S. C. and Pindera, M-J., "Stress and Plastic Strain Fields During Unconstrained and Constrained Fabrication Cool Down of Fiber Reinforced IMC's", J. Composites Engineering, (accepted for publication).
- Cantonwine, P. E. and Wadley, H. N. G., "The mechanical response of sintered alumina bundles", Ceramic Matrix Composite Symposium Proceedings, American Ceramic Society, Cincinnati, OH, May 3-6, 1998.
- Edge, A. C., Laufer, G. and Krauss, R. H., "Temperature Field Imaging Using a laser-Pumped Thermographic Phosphor", Conference on lasers and Electro-Optics, May 18-23, Baltimore, MD, 1997.
- Hammond, V. H., Elzey, D. M. and Wawner, F. E., "The Influence of Plasma Composition on Quality of Spray Deposited Nickel Aluminide Foils", Scripta Materialia, (accepted for publication).
- Herakovich, C. T. and Aboudi, J. "Thermal Effects in Composites", (invited review paper to be published in Thermal Stresses Vol. 5, R. Hetnarski, Ed., copy-ready manuscript has been submitted).
- Herakovich, C. T. & Baxter, S. C. "Influence of Pore Geometry on the Effective Response of Porous Media", (submitted for publication).
- Herakovich, C. T. & Mirzadeh, F., (1997), "Thermal-Mechanical Response of Stiffened Composite Cylinders", Applied Mechanics in the Americas, Vol. 5: Mechanics of Fluids, Thermal Problems, Optimization and Control, Experimental and Numerical Methods, Biomechanics, Applications, (M. Rysz, L. A. Godoy, L. E. Suarez, Eds.), The University of Iowa, Iowa City, IA.
- Hersh, C. L. and Herakovich, C. T., "Local Effects in Stiffened Composite Tubes under Generalized Plane Deformation", J. Composite Materials, (accepted for publication).
- Laufer, G. Rotchford, N. B. and Krauss, R. H., "Temperature Field Visualization in Conducting Solids Using Thermographic Phosphors", American Journal of Physics, May, 1997, pp. 447-449.
- Laufer, G., Westring, B. D. and Marino, R. P., "Modified Spin Filter for Noise Reduction in Aerodynamic Imaging", Optics and Laser Technology, Vol. 29, 1997, pp. 159-163.
- Marino, R. Westring, B. Laufer, G. and Krauss, R. H., "Optical Full Field Surface Temperature and Strain Measurements", (submitted for publication).

- Marino, R., Westring, B., Laufer, G, and Krauss, R. H.,. "Optical full Field Surface Temperature and Strain Measurements", AIAA 97-0385, AIAA 35th Aerospace Sciences Meeting, Reno, NV, Jan. 6-9, 1997.
- McGarry, T. D., Hammond, V. H., Pindera, M.-J. and Wawner, F. E., "Evaluation of Thermal Barrier Coatings on SCS-6 Fibers in Ti14Al21Nb Composites," Proceedings of the First International Conference on Composites Engineering, edited by David Hui, 1994, pp. 559-560.
- McGarry, T., Pindera, M-J, and Wawner, F., (1995), "Evaluation of Reaction Barrier Compensating Coatings on SCS-6 Fibers in Ti24Al11Nb Composites," Composites Engineering, 5 (7), pp. 951-974.
- Pindera, M-J., Arnold, S. M., and Williams, T. O., "Thermoplastic Response of Metal Matrix Composites with Homogenized and Functionally Graded Interfaces," Composites Engineering, Vol. 4, No. 1, 1994, pp. 129-145.
- Prins, R., Laufer, G., Krauss, R. H. and Narasimhan, (1995), "An Optical Method for Simultaneous Measurement of Surface Strain and Temperature", AIAA Paper #AIAA 95-0482, AIAA 33rd Aerospace Sciences Meeting, Reno, NV, Jan. 9-12.
- Salzar, R. S. and Pindera, M-J., "Optimization of Functionally Graded Metal Matrix Composite Tubes," in Proc. 10th ASCE Engineering Mechanics Conference, S. Sture (Ed.), pp. 1195-1198, 1995. ASCE, New York.
- Salzar, R. S., Pindera, M-J., and Barton, F. W., "Elastic/Plastic Analysis of Layered Metal Matrix Composite Cylinders. Part I: Theory," Journal of Pressure Vessel Technology, Vol. 118, No. 1, 1996, pp. 13-20.
- Salzar, R. S., Pindera, M-J., and Barton, F. W., "Elastic/Plastic Analysis of Layered Metal Matrix Composite Cylinders. Part II: Applications," Journal of Pressure Vessel Technology, Vol. 118, No. 1, 1996, pp. 21-26.
- Sankurathri, A., Baxter, S., and Pindera, M-J., "The Effect of Fiber Architecture on the Inelastic Response of Metal Matrix Composites with Interfacial and Fiber Damage," in Damage and Interfacial Debonding in Composites, G. Z. Voyiadjis and D. H. Allen (Eds.), pp. 235-257, 1996. Elsevier Science B.V., The Netherlands.
- Westring, B. D., Laufer, G. and Marino, R. P., "Modified Spin Filter for Digital Moiré Processing" (submitted for publication).
- Williams, T. O. and Pindera, M-J., "Convergence Rates of the Method of Successive Elastic Solutions in Thermoplastic Problems of a Layered Concentric Cylinder," in Engineering, Construction, and Operations in SPACE IV, R. G. Galloway and S. Lokaj, Eds., pp. 348-357, 1994. ASCE, New York.
- Williams, T. O. and Pindera, M-J., "An Analytical Model for the Inelastic Axial Shear Response of Unidirectional Metal Matrix Composites," International Journal of Plasticity, Vol. 13, No. 3, 1997, pp. 261-289.
- Williams, T. O. and Pindera, M-J., "TMF Modeling of Advanced Metal Matrix Composites in the Presence of Microstructural Details," 3Materials Science and Engineering, Vol. A200, No. 1-2, 1995, pp. 156-172.
- Yu, S. C. and Elzey, D. M., "Processing and Characterization of an hybrid Fiber Reinforced Ni Aluminide", Materials Science and Engineering, 1997.

Books:

- Herakovich, C. T., Mechanics of Fibrous Composites, John Wiley and Sons, Inc. (available Nov. 1997).

Presentations:

- Baxter, S. C. and Pindera, M-J, "Mechanical Response of Functionally Graded MMC Tubes with Fiber Damage to Torsional Loading", 3rd International Conference on Composites Engineering ICCE/3, New Orleans, 1996.
- Cantonwine, P. E. and Wadley, H. N. G., "The mechanical response of sintered alumina bundles", Ceramic Matrix Composite Symposium Proceedings, American Ceramic Society, Cincinnati, OH, May 3-6, 1998.
- Cantonwine, P. E. and Wadley, H. N. G., "A Non-conventional, Affordable Process for High Temperature Tow-based Composites", Aeromat 96, Am. Soc. Metals, Dayton, OH, June 6-9, 1996.
- Gan, H., Orozco, C. E. and Herakovich, C. T., "Shear Compatible Method of Cells for Micromechanics), USNCAM13, University of Florida, June, 1998
- Hammond, V. H., Elzey, D. M. and Wawner, F. E., "Creep Behavior of Nextel 610 Tows and Hybrid Fibers," Virginia Academy of Science Meeting, May 28, 1998.
- Hammond, V. H., Elzey, D. M. and Wawner, F. E., "Influence of Plasma Composition on Ni3Al Foil Quality," Materials Science Section, Meeting of the Virginia Academy of Sciences, May 22, 1997.
- Hammond, V. H., Elzey, D. M. and Wawner, F. E., "Plasma Spray Deposited Fiber-Rein forced Ni3Al," Department of Materials Science, University of Erlangen-Nürnberg, Erlangen, Germany, Oct. 18, 1996.
- Hammond, V. H., Elzey, D. M. and Wawner, F. E., "Plasma Spray Deposited Fiber-Reinforced Ni3Al," Institute für Metallkunde, Universität Stuttgart and Max Planck Institute für Metallkunde, Stuttgart, Germany, Oct. 17, 1996.
- Hammond, V. H., Elzey, D. M. and Wawner, F. E., "Plasma Spray Deposited Fiber-Reinforced Ni3Al," Department of Materials Science and Engineering, University of Surrey, Guildford, England, Oct. 15, 1996.
- Hammond, V. H., Elzey, D. M. and Wawner, F. E., "Plasma Spray Deposited Fiber-Reinforced Ni3Al," School of Metallurgy and Materials, University of Birmingham, Birmingham, England, Oct. 11, 1996.
- Herakovich, C. T., Baxter, S. C. and Heasley, S., "Influence of Pore Geometry on the Effective Response of Porous Media", McNU'97, Northwestern Univ. June, 1997.
- Herakovich, C. T. & Mirzadeh, F., (1997), "Thermal-Mechanical Response of Stiffened Composite Cylinders", PACAM V, San Juan, Puerto Rico, Jan. 1997.
- Herakovich, C. T., Schroedter, R. D., III, Gasser, A. and Guitard, L., "Mesoscale Damage Modeling of Carbon-Polyimide Composites", McNU'97, Northwestern Univ. June, 1997.

- McGarry, T. D., Hammond, V. H., Pindera, M-J., and Wawner, F. E., "Evaluation of Thermal Barrier Coatings on SCS-6 Fibers in Ti14-Al21-Nb Composites," Proc. ICCE/1, August 28-31, 1994, New Orleans, LA.
- McGarry, T., Gundel, D. and Wawner, F., "The Effect of Thermal Exposure on Yttria Coated SCS-6 Fibers," presented at the 1st SES-ASME-ASCE Joint Meeting on Functionally Graded Interfaces and Advanced Composite Materials, June 6-9, 1993, Charlottesville, VA.
- McGarry, T., Hammond, V., Pindera, M-J. and F. Wawner, "Evaluation of Thermal Barrier Coatings on SCS-6 Fibers in Ti14Al21Nb Composites," presented at the 1st International Conference on Composites Engineering, ICCE/1, August 28-31, 1994, New Orleans, LA
- McGarry, T., Pindera, M-J. and F. Wawner, "Evaluation of Compliant Layer Diffusion Barrier Coatings on SCS-2 Fibers in Ti24Al11Nb Composites," presented at the 2nd International Conference on Composites Engineering, ICCE/2, August 21-24, 1995, New Orleans, LA
- Roerden, A. M. and Herakovich, C. T., "Inelastic Response of Porous Composites", USNCAM13, University of Florida, June, 1998
- Roerden, A. M. and Herakovich, C. T., "Inelastic Response of Porous, Hybrid Fiber Composites", ASME, IMECE, Nov., 1998.
- Salzar, R. S. (1995), "Plastification Optimization of Layered MMC Cylinders Through Functionally Graded Architectures," Symposium on Functionally Graded Materials (ICCE/2), August 21-24, 1995, New Orleans.
- Williams, T. O. and Pindera, M-J. (1994), "Convergence Rates of the Method of Successive Elastic Solutions in Thermoplastic Problems of a Layered Concentric Cylinder,"
- Williams, T. O. and Pindera, M-J. (1994), SPACE'94, Fourth Int. Conference on Engineering, Construction, and Operations in Space, Albuquerque, New Mexico, Feb 26 - March 3, 1994.
- Williams, T. O. and Pindera, M-J., "TMF Modeling of Advanced Metal Matrix Composites in the Presence of Microstructural Details," TMS/ASM Symposium on Mechanisms and Mechanics of MMC Fatigue, October 2-6, 1994, Rosemont, Illinois.
- Williams, T. O. (1995), "Longitudinal Shear Response of Unidirectional IMC's with Interfacial Layers," Symposium on Functionally Graded Materials (ICCE/2), August 21-24, 1995, New Orleans.
- Yu, S. C. and Elzey, D. M., "Processing and Characterization of an hybrid Fiber Reinforced Ni Aluminide", Symposium on Advances in Synthesis and Processing of Metal and Ceramic Matrix Composites", TMS Annual Meeting, Orlando, FL, Feb. 9-13, 1997.

AWARDS

- Paul E. Cantonwine was selected as a 1996-97 Virginia Space Grant Fellow
- Vince H. Hammond was selected as a 1998-99 Virginia Space Grant Fellow

ADVISORY BOARD

Major John Pernot
HQUS AFA/DFEM
2354 Fairchild Drive
Suite 6H2
US Airforce Academy, CO 80840-6240

Dr. Frederick C. Polhemus, Jr.
United Technologies Pratt & Whitney
P.O. Box 109600
West Palm Beach, FL 33410-9600

Major Brian Sanders
Dept. of the Air Force
110 Duncan Avenue, Suite B115
Bolling AFB, DC 20332-0001

Mr. James P. Sorensen
Technical Manager
3M Center
Bldg 60-1N-01
St. Paul, MN 55144
Ph: (612)736-9892; FAX: (612)736-0431
Email: jpsorensen@mmc.mmmg.com

Capt. Charles H. Ward
AFOSR/NC
110 Duncan Avenue, Suite B115
Bolling AFB, DC 20332-0001
Ph: (202)767-4963; FAX: (202)767-4961

Dr. James C. Williams
General Electric Aircraft Engines
One Neumann Way, MD H85
Cincinnati, OH 45215-6301
Ph: (513)243-4531; FAX: (513)243-3526

EXECUTIVE SUMMARIES

Executive summaries of the technical accomplishments during the grant period are presented in the following pages according to the schedule below:

PROCESSING AND PROPERTIES OF A-PA HYBRID FIBERS

Paul E. Cantonwine and Haydn N.G. Wadley

Executive Summary

After the decision was made to focus this URI on extending the use temperatures of metal matrix composites via the hybrid fiber processing approach, it was our responsibility to provide enough alumina-porous alumina (A-PA) hybrid fiber to support the groups efforts. A schematic of the hybrid fiber approach is shown in figure 1. Within six months a lab scale fiber line (see figure 1a) was developed which enabled us to manufacture over 5000 feet of fiber in one week.

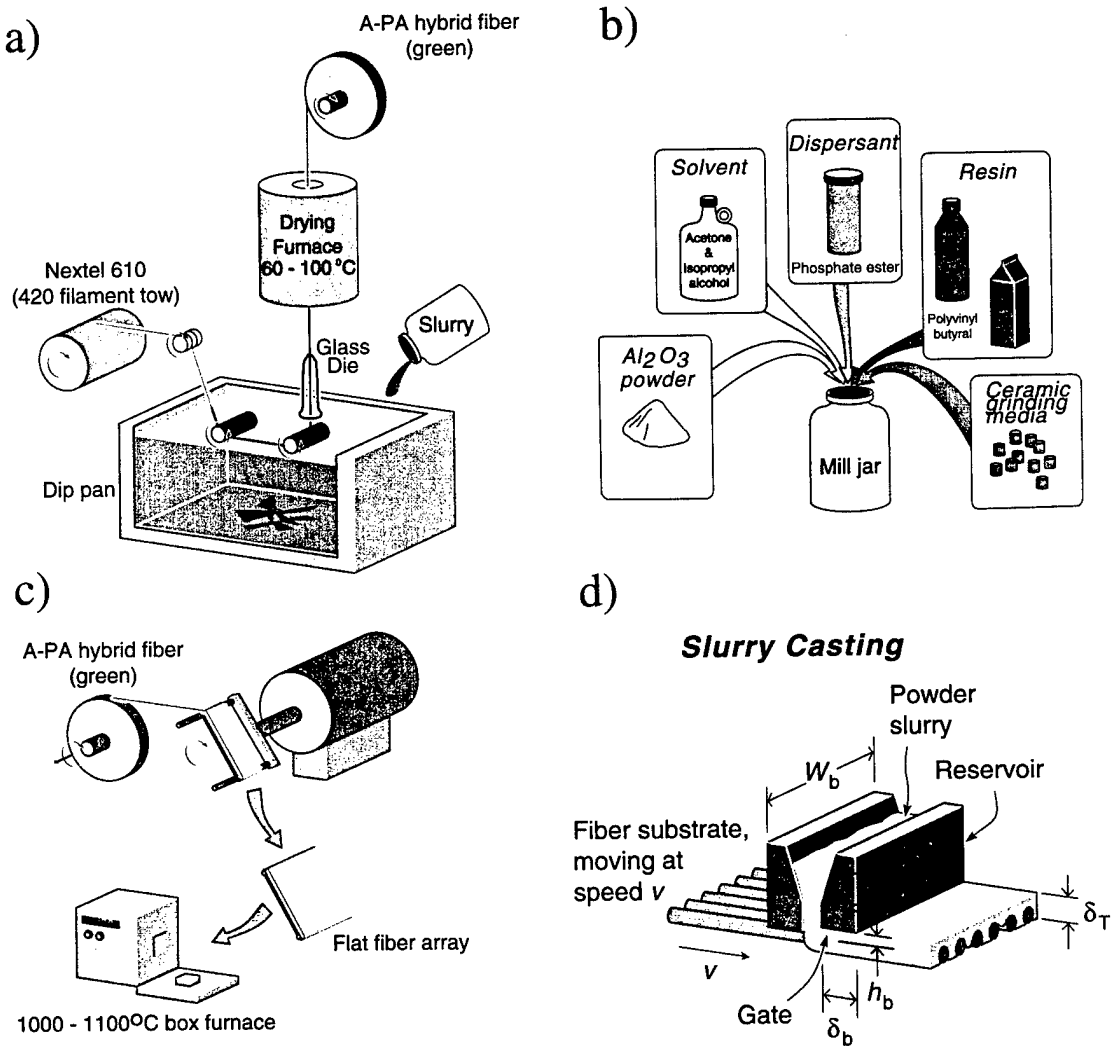

Figure 1 A schematic of the hybrid fiber processing approach: a) A-PA hybrid fiber line b) composition of slurry poured into dip pan c) fiber winding and sintering d) slurry casting of metal matrix

The desired operating temperatures of these materials are between 800 and 1000 °C. Therefor, understanding the effects of high temperature aging on the mechanical properties is essential. Figure 2 shows the important microstructural features of the A-PA hybrid fiber. When heat is applied, three different sintering phenomena will occur simultaneously. First the powder/powder contacts will grow; second, the powder/filament contacts will grow and third, the filament/filament contacts will grow. Our approach was to isolate the effect of each sintering phenomena in order to understand how they related to mechanical properties. Currently, we will concentrate on describing the effect of the filament/filament contacts on the room temperature tensile properties of the alumina bundles and A-PA hybrid fiber. We will also briefly discuss the effects of the powder/powder and powder/filament contacts.

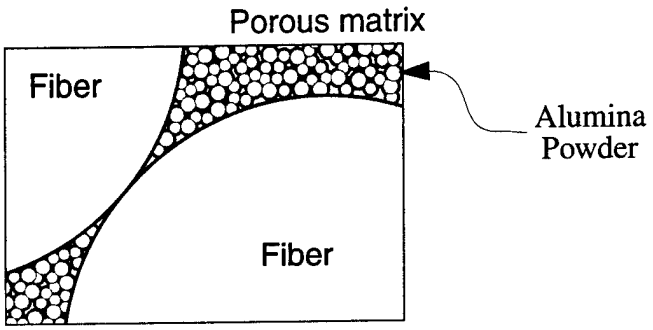

Figure 2 A porous alumina matrix reinforced with alumina filaments

Uninfiltrated bundles were heat treated to investigate the effect of filament/filament sintering on the mechanical response of alumina bundles. Both the single filament and bundle strengths decreased with sintering temperature. Fractography of the single filament fractures indicated a dramatic change in the defect population; at the higher temperatures more filaments failed from weld-line defects caused by filament/filament sintering.

Using the single filament strengths from the heat treated bundles, ideal bundle predictions were compared to the measured bundle response. At the lower temperatures, the ideal bundle model predicted the bundle response, but dramatically overpredicted the failure stress and strain after high temperature aging. Two reasons for the overprediction are proposed. First, the ideal bundle model assumes each filament is independent from its neighbor, however when filaments are bonded together this assumption is no longer valid. Second, differences in the fracture surfaces indicated the stress distribution around the weld-line at failure was different in the single filament tests (filaments pulled apart) compared to the bundle tests (filaments in contact). This is an indication that the filaments may be weaker when they are in contact compared to when they have been pulled apart.

In addition, it is believed that in this oxide/oxide system, the interfacial shear strength is controlled by the shear strength of the powder/filament contacts. The interfacial shear strength is a function of the size and number of the powder/filament contacts, and was varied by varying the density of the matrix and the aging temperature. The results indicated that with a low interfacial shear strength the filament/filament bonding defects dominated but as the shear strength increased, local load sharing effects began to emerge.

Processing and Properties of A-PA Hybrid Fibers

University of Virginia B.3 Paul E. Cantonwine

Outline

- Introduction
  - Motivation; Materials; Procedures
- Single Filament Properties
  - Weibull Parameters; Fractography; Grain size
- Bundle Properties
  - Stress/Strain Measurements; Ideal Bundle Predictions; Fractography
- CMC Properties

Schematic of A-PA Hybrid Fiber Microstructure

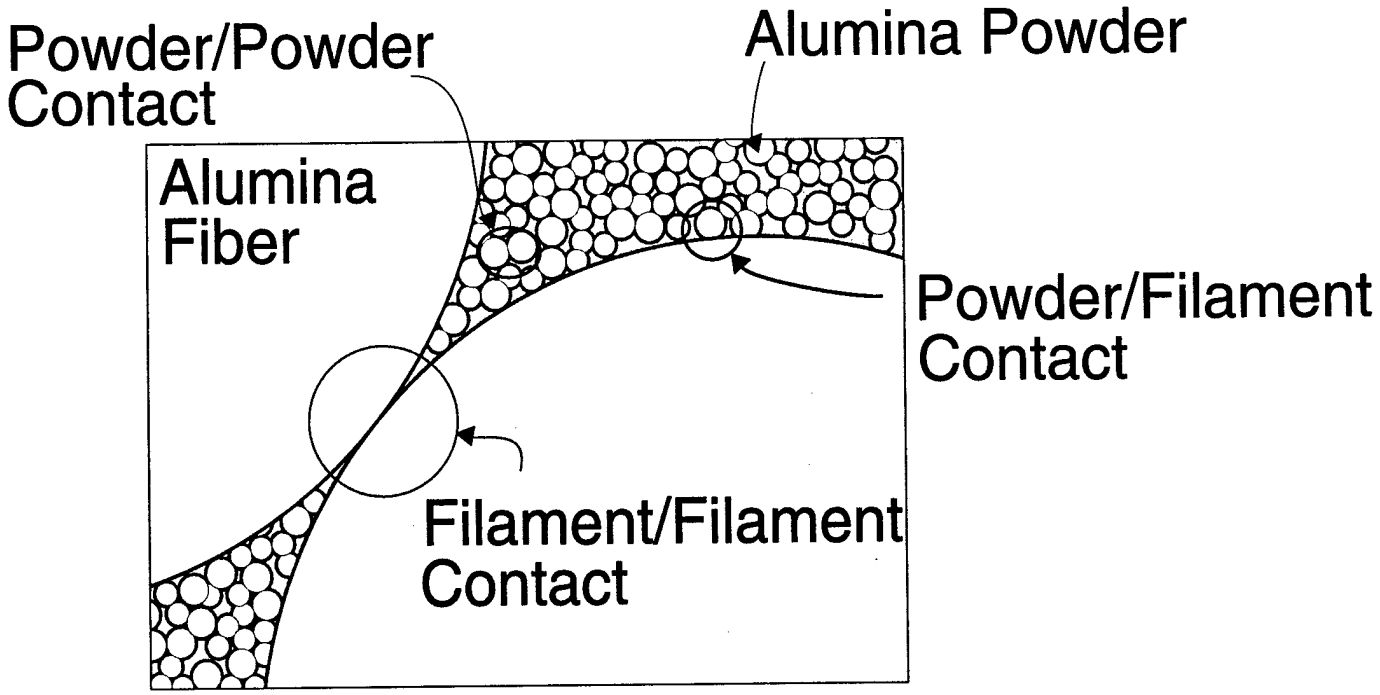

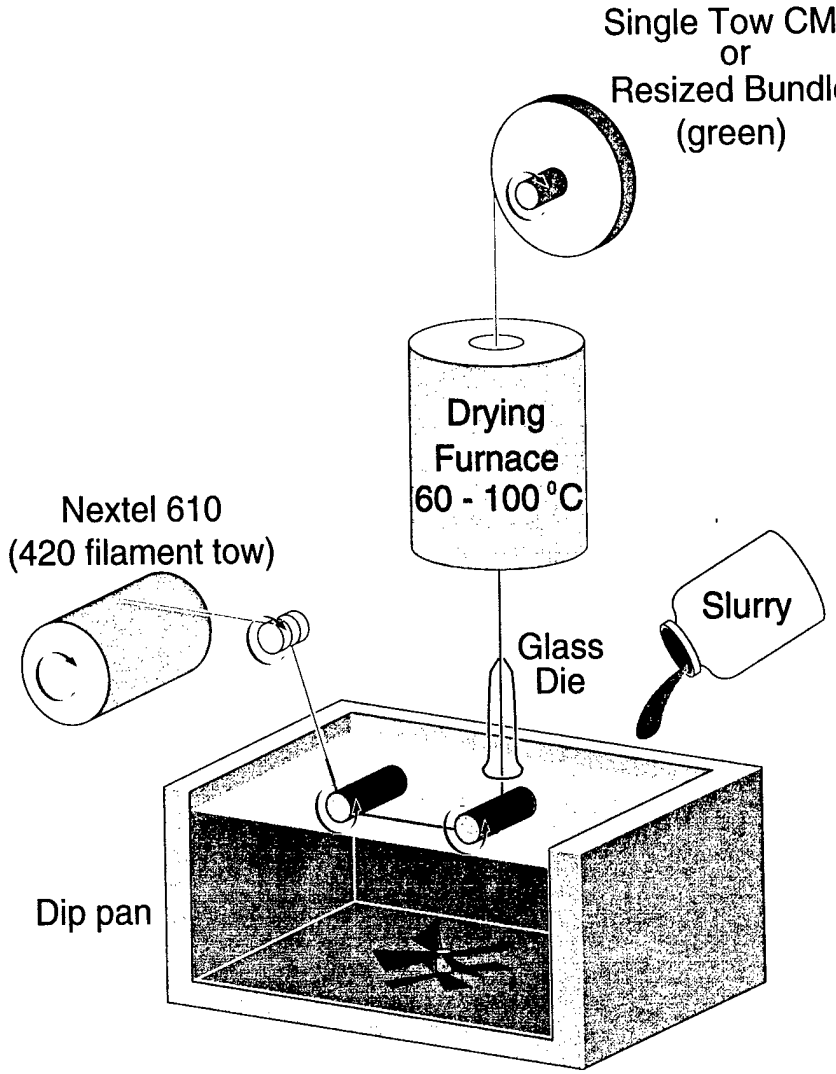

2349 hybrid fiber p cantonwine ipm 9/96

In-line Sintering

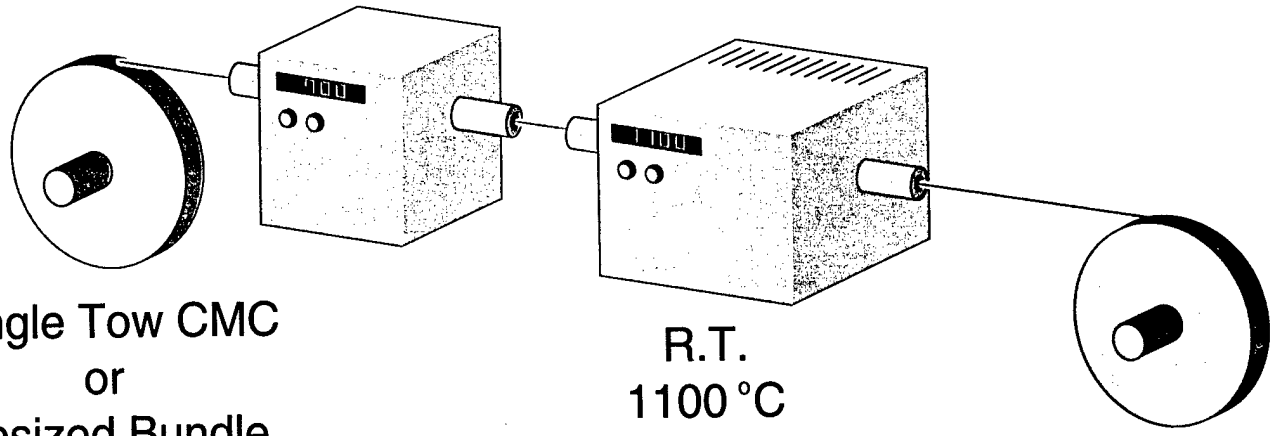

Single Tow CMC
or
Resized Bundle
(green)

R.T.
1100 °C
1200 °C
1300 °C
1350 °C
1400 °C
1450 °C

Pick-up Reel
(1 ft/min)

2349 inline p cantonwine ipm 9/96

Single filament strengths as a function of aging temperature

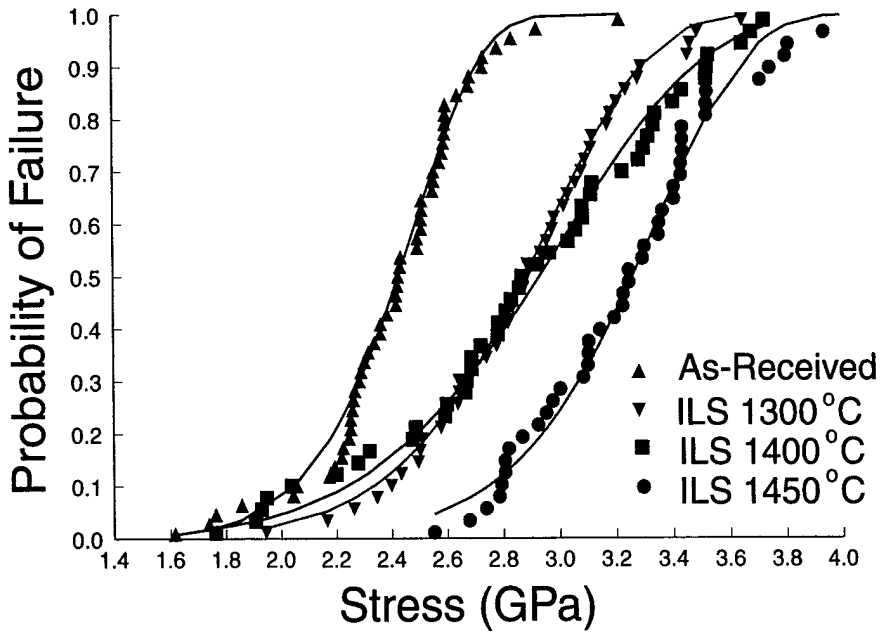

$$P_f = 1 - \exp\left[\frac{L}{L_o}\left(\frac{S}{S_o}\right)^m\right]$$

Heat Treatment	S_o (GPa)	m
As-Received	3.37	11.0
1100°C	3.3	7.1
1200°C	3.3	7.0
1300°C	3.09	7.0
1350°C	3.1	8.1
1400°C	3.0	9.0
1450°C	2.51	11.0

Fractography; Internal Defects

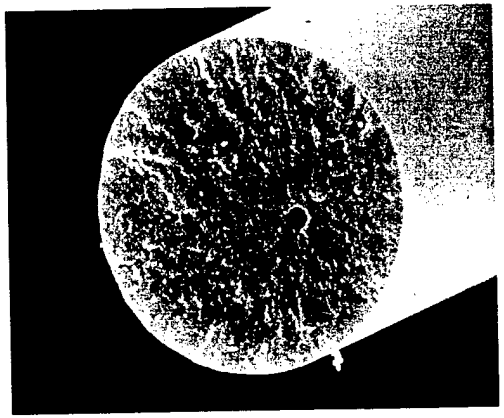

Spherical Pore

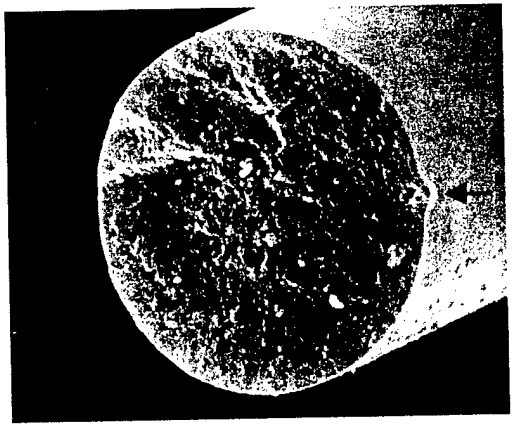

Porosity

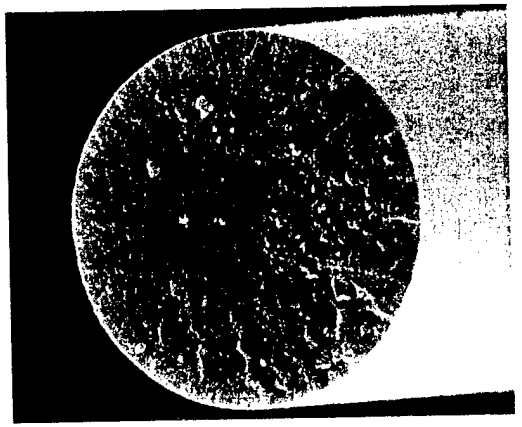

Non-Geometric

10 μm

Fractography; Surface Defects

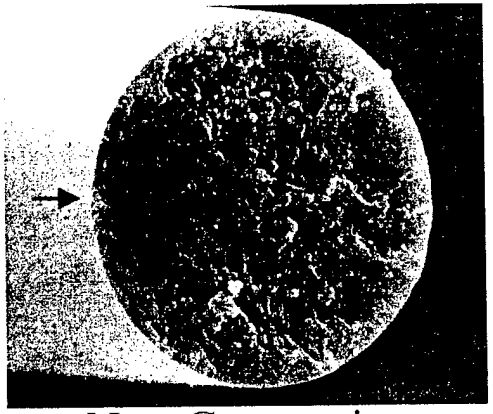

Non-Geometric

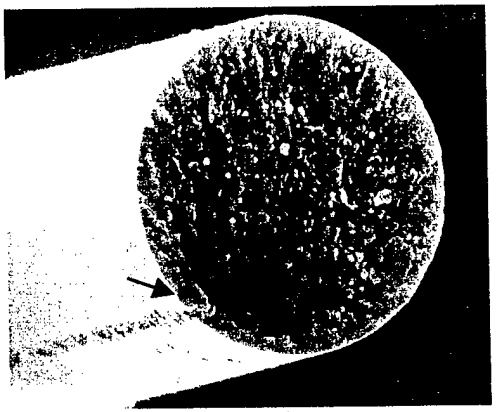

Weld-line

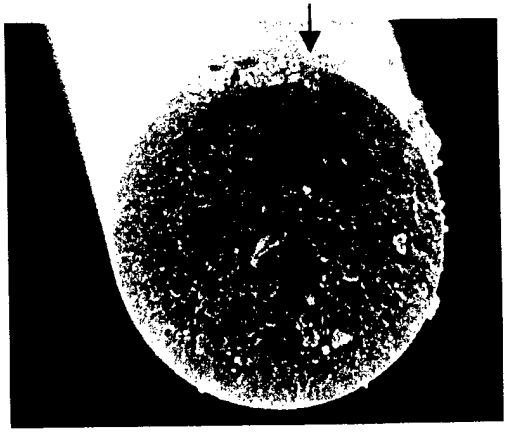

Blister

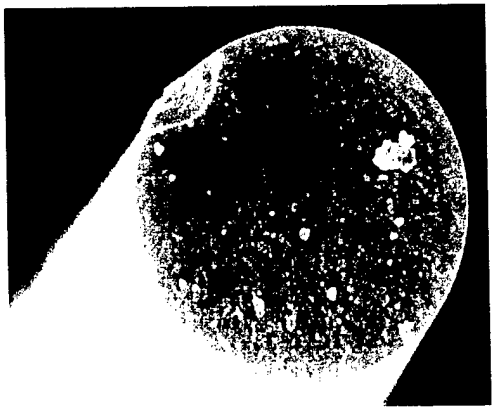

Crack

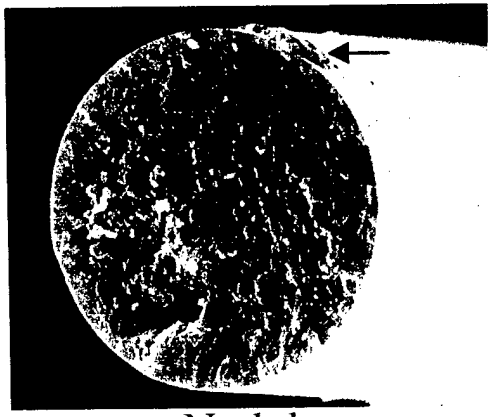

Nodule

10 µm

Defect Distribution: As-received

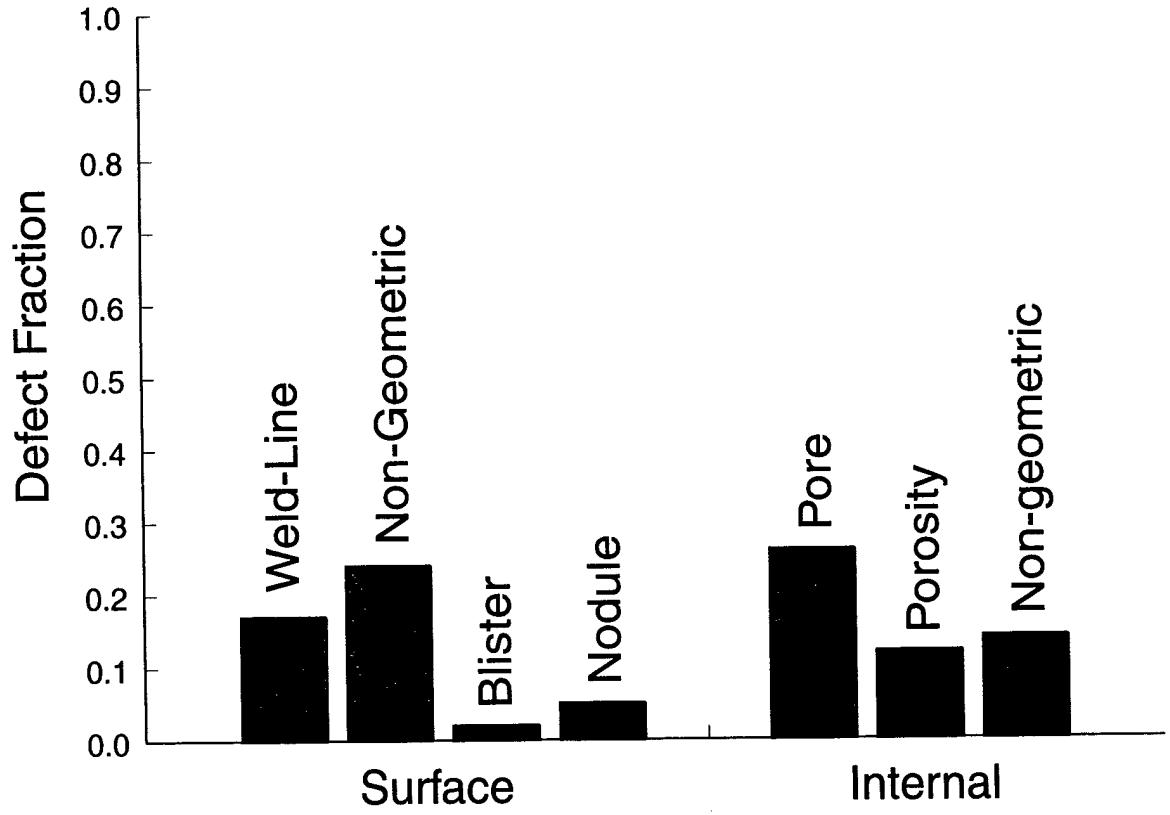

Defect Distribution; ILS 1450 °C

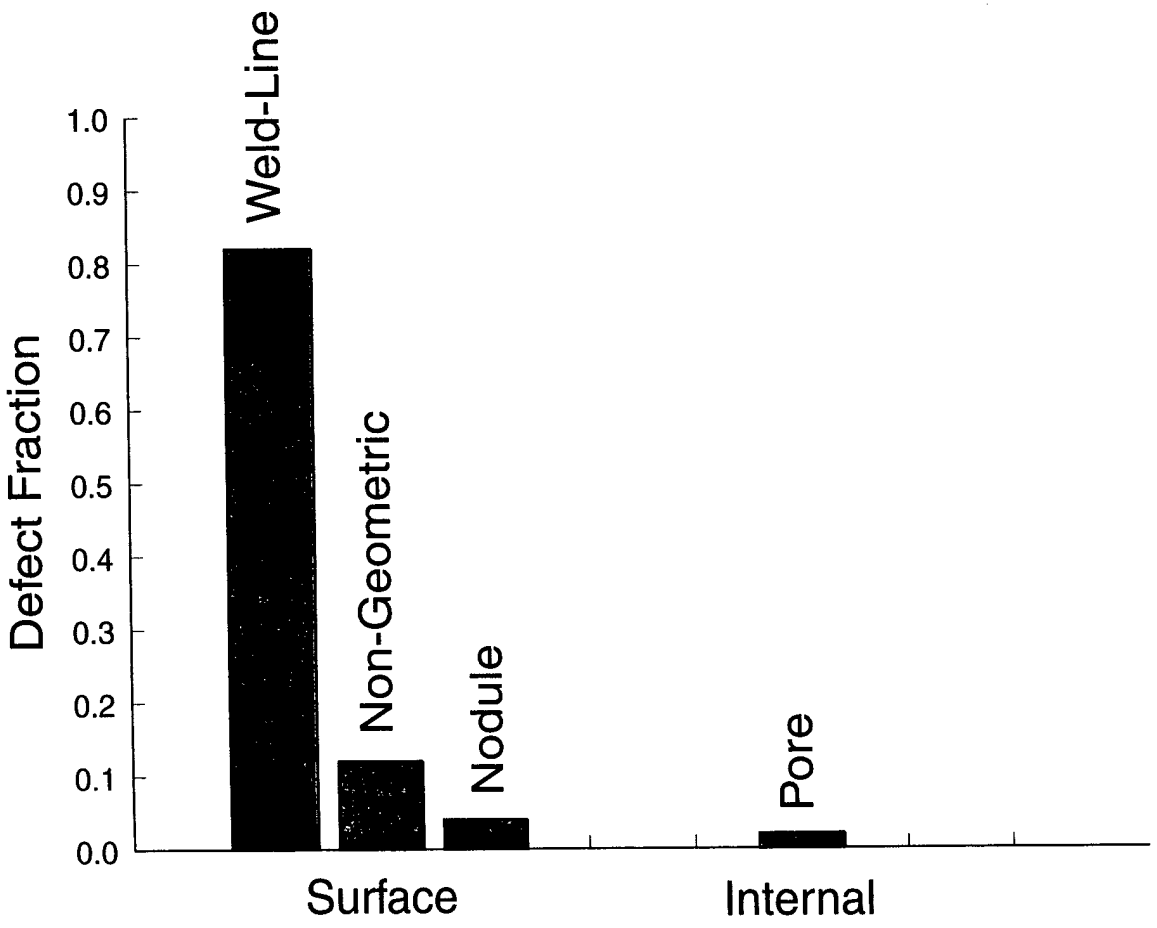

Grain Size

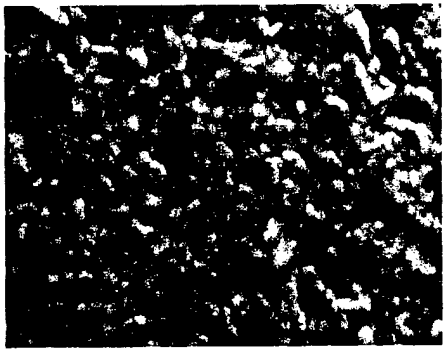

As-Received (63 nm)

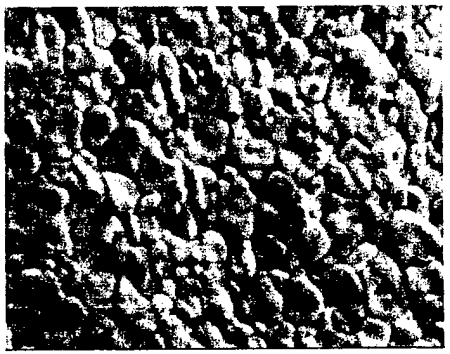

ILS 1300 °C (74 nm)

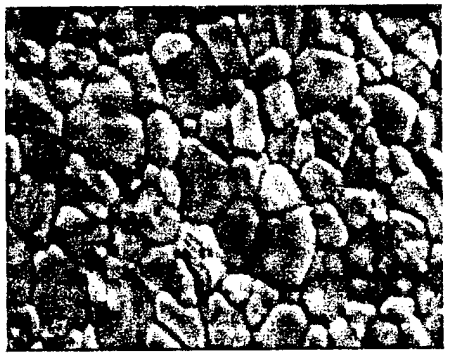

ILS 1400 °C (90 nm)

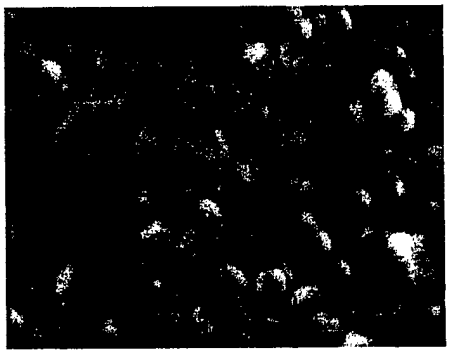

ILS 1450 °C (98 nm)

Heat Treatment	Grain Size (nm)
As-Received	63
ILS 1100 °C	69
ILS 1200 °C	68
ILS 1300 °C	74
ILS 1350 °C	76
ILS 1400 °C	90
ILS 1450 °C	98

200 nm

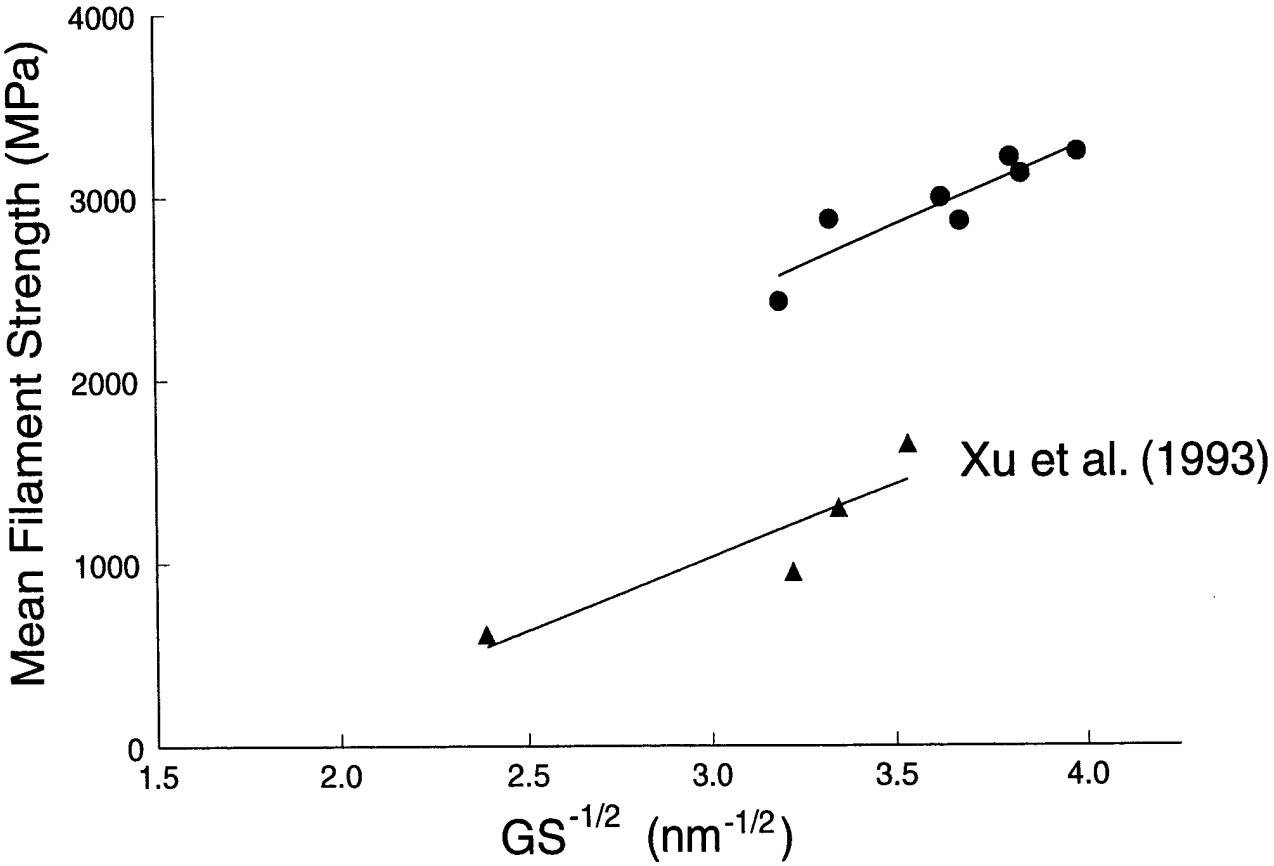
Mean Filament Strength (MPa)
4000
3000
2000
1000
0
1.5
2.0
2.5
3.0
3.5
4.0
GS-1/2 (nm-1/2)
Xu et al. (1993)

Tensile Testing Apparatus

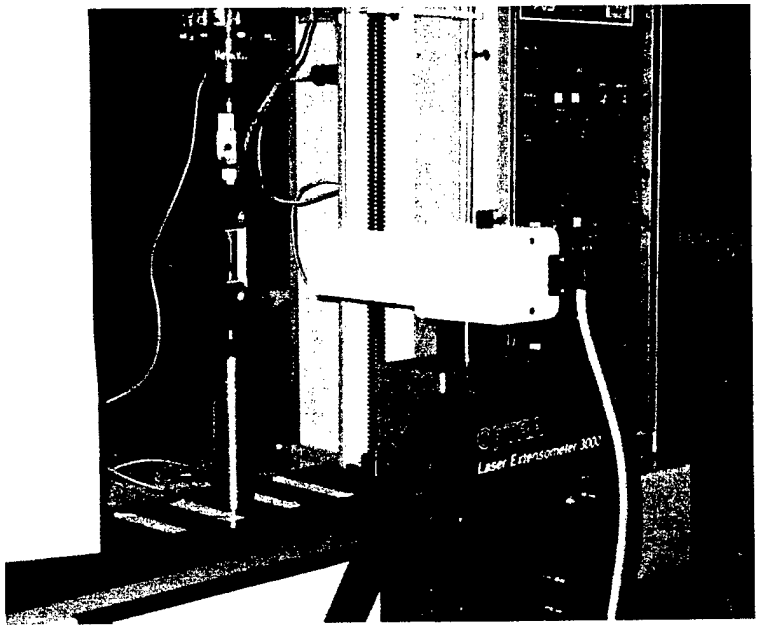

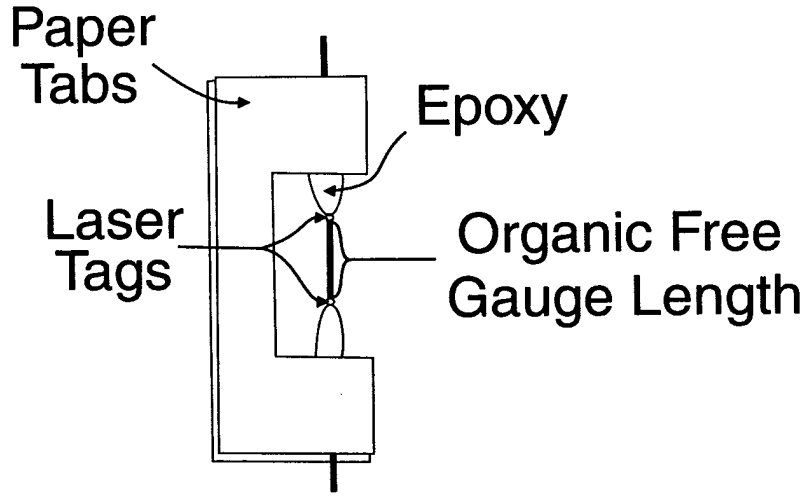

Stress/Strain Response of Alumina Bundles

As-Received

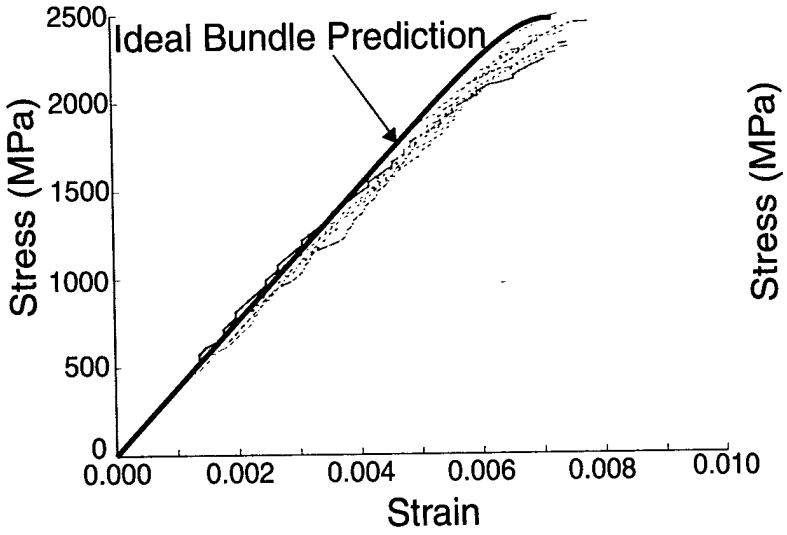

ILS 1300° C

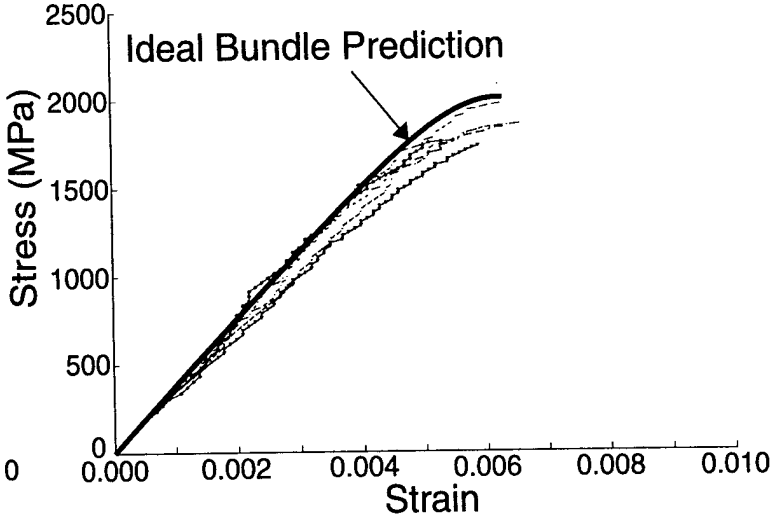

Stress/Strain Response of Alumina Bundles

ILS 1400° C

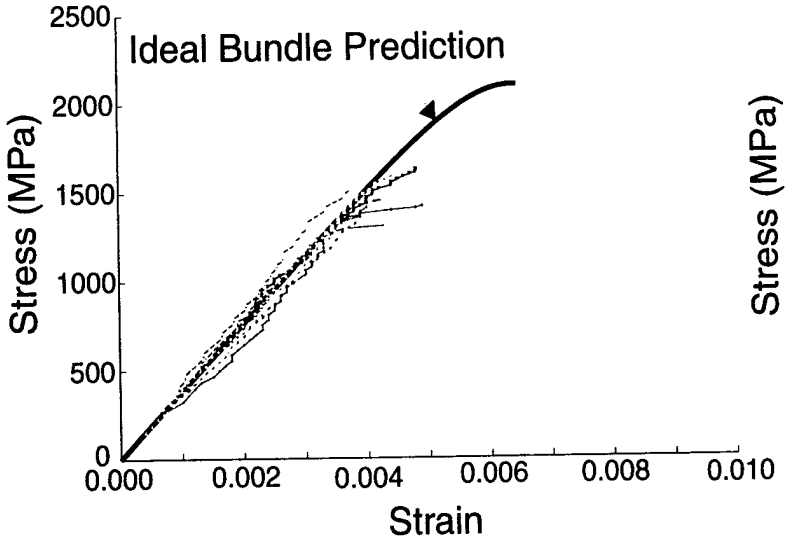

ILS 1450° C

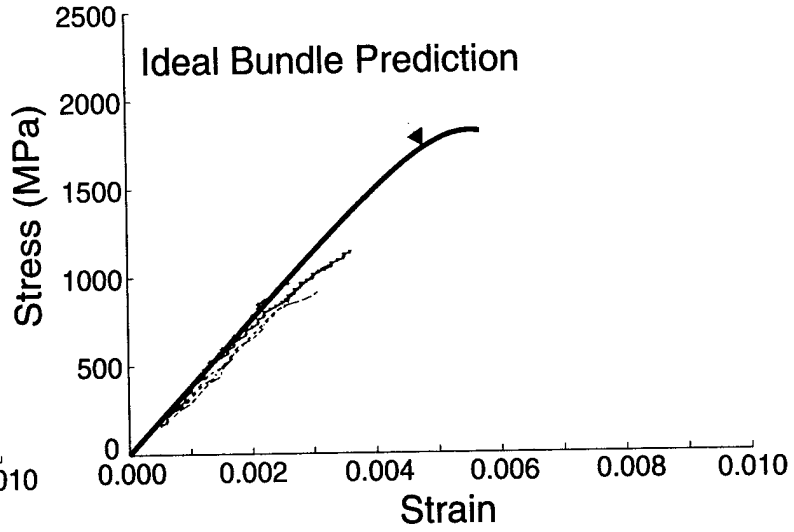

Ideal Bundle Model

- Assumptions
  - Large number of filaments; > 200 (Phoenix and Raj)
  - Filaments are perfectly aligned
  - Global load sharing
  - Filaments follow weakest link statistics (Weibull)
  - Filaments fail independent of neighbors

Ideal Bundle Model

$$\sigma_b = \sigma_f (1 - P_f)$$

$\sigma_f = E_f \varepsilon$ Hooke's Law

$P_f = 1 - \exp\left[\frac{L}{L_o}\left(\frac{\sigma}{\sigma_o}\right)^m\right]$ Weibull Statistics

$$\sigma_b = E_f \varepsilon \exp\left[\frac{L}{L_o}\left(\frac{E_f \varepsilon}{\sigma_o}\right)^m\right]$$

Defect Distribution: As-Received

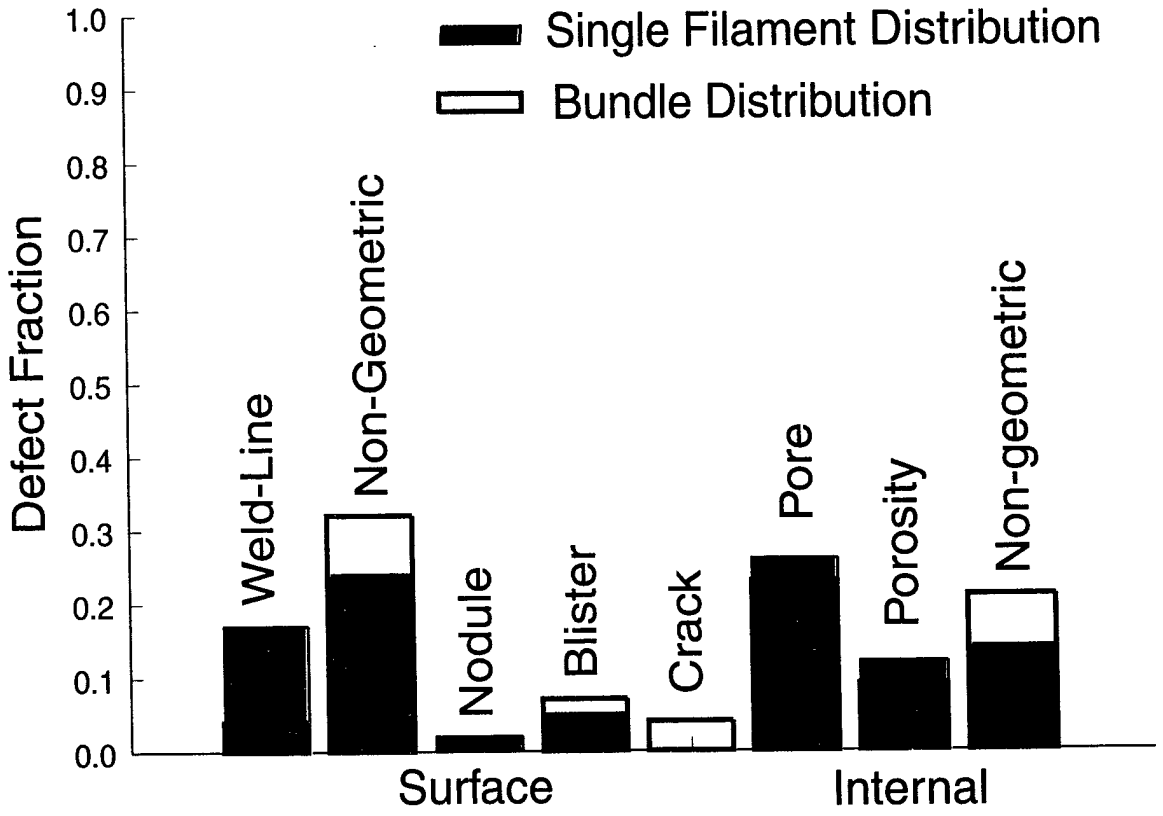

Defect Distribution: ILS 1450 °C

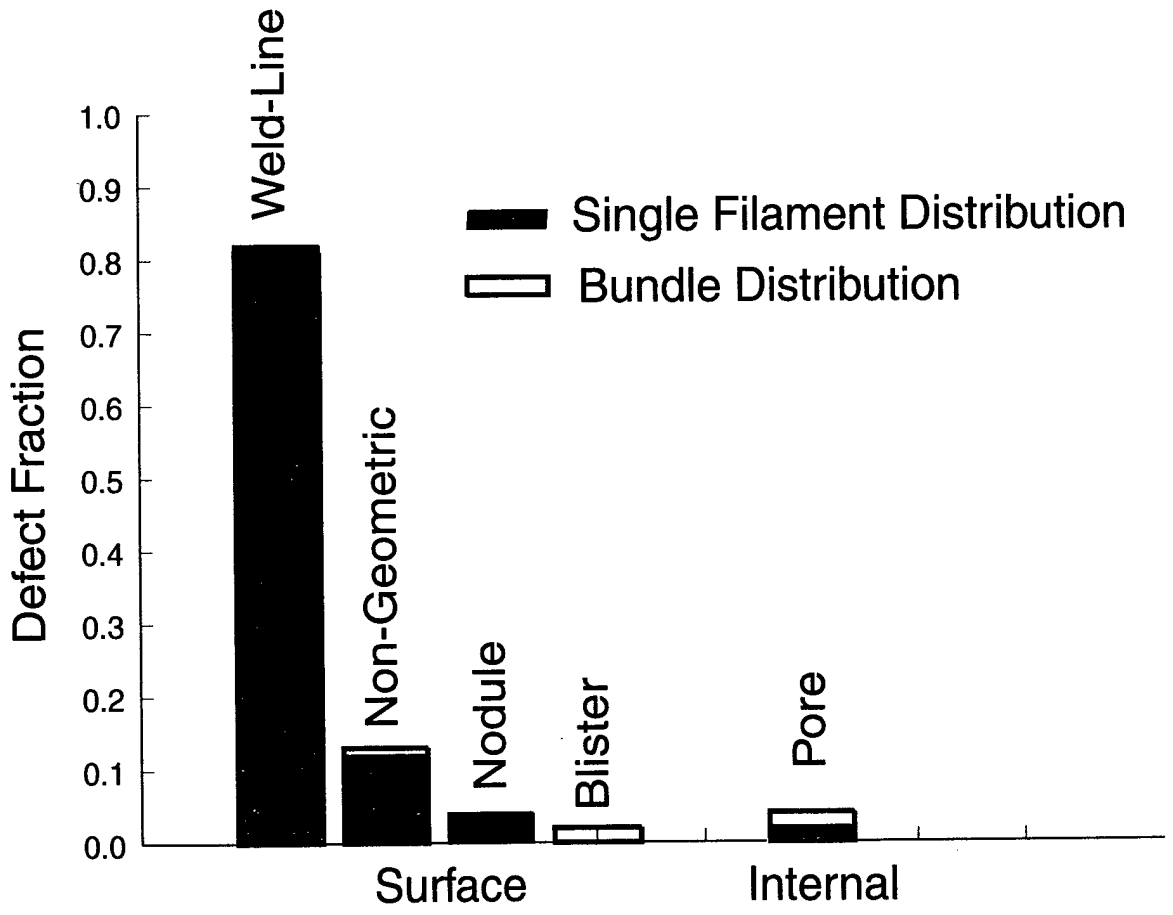

Fractography: Filament Clusters

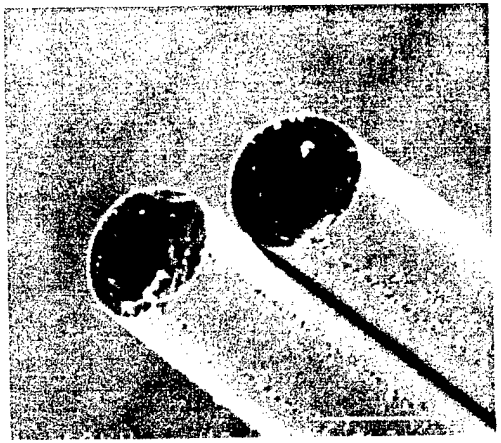

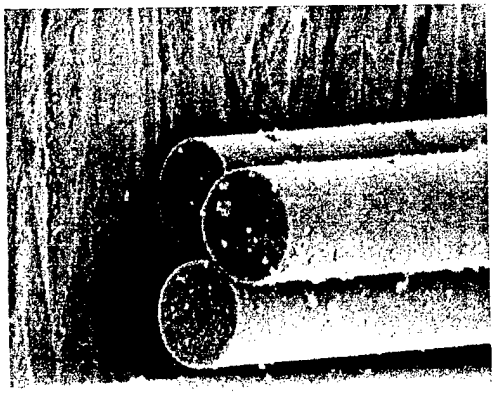

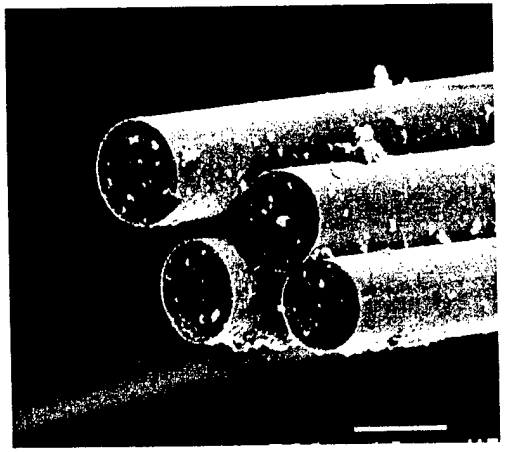

Monte Carlo Simulations: Filament Cluster Effects

- Assumptions
  - Filament strengths are characterized from single filament tests.
  - Filament clusters fails when the weakest filament fails.
  - Worst Case Scenario: 80% of the filaments are in one cluster.

Monte Carlo Simulations: ILS 1450 °C

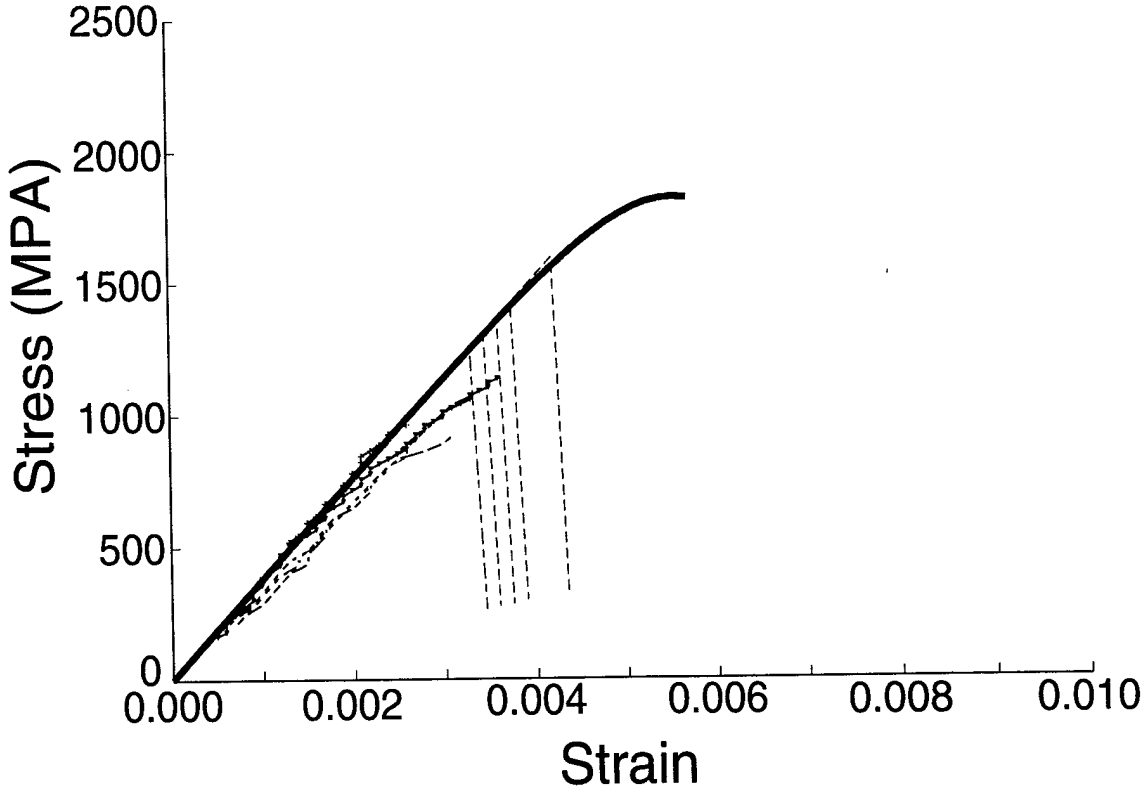

Fractography: Weld-Line Defects

Bundle Fracture

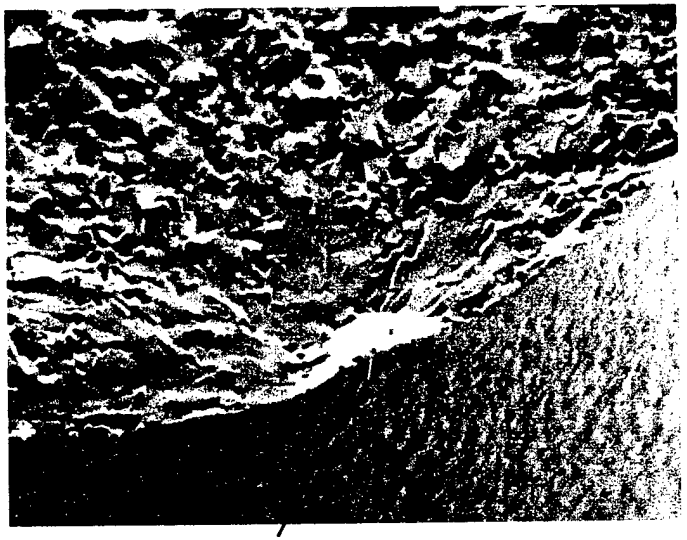

Focal Point
and
Weld-Line

Single Filament Fracture

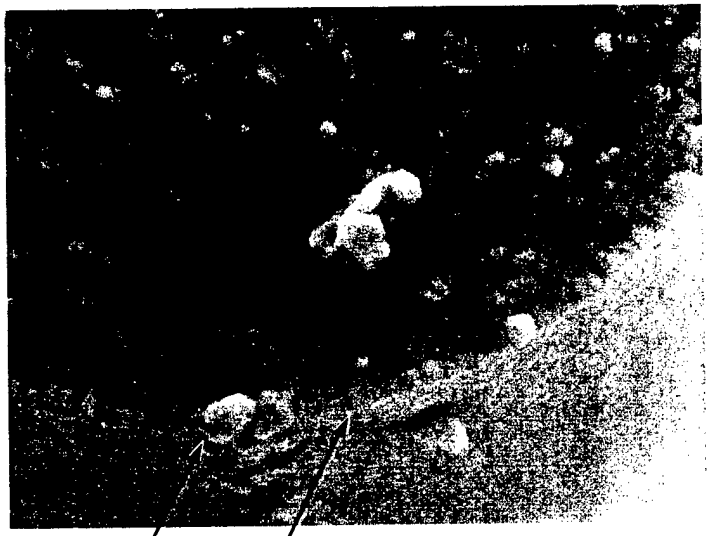

Interfacial strength controlled by the shear strength of the powder/filament contacts.

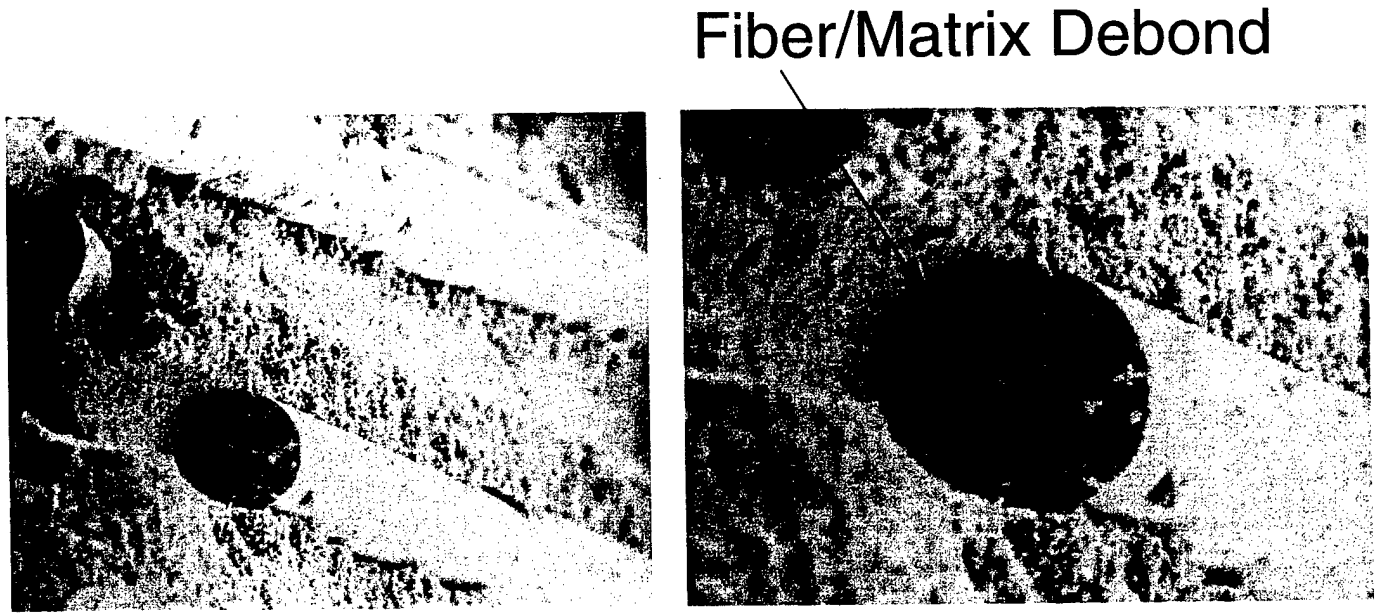

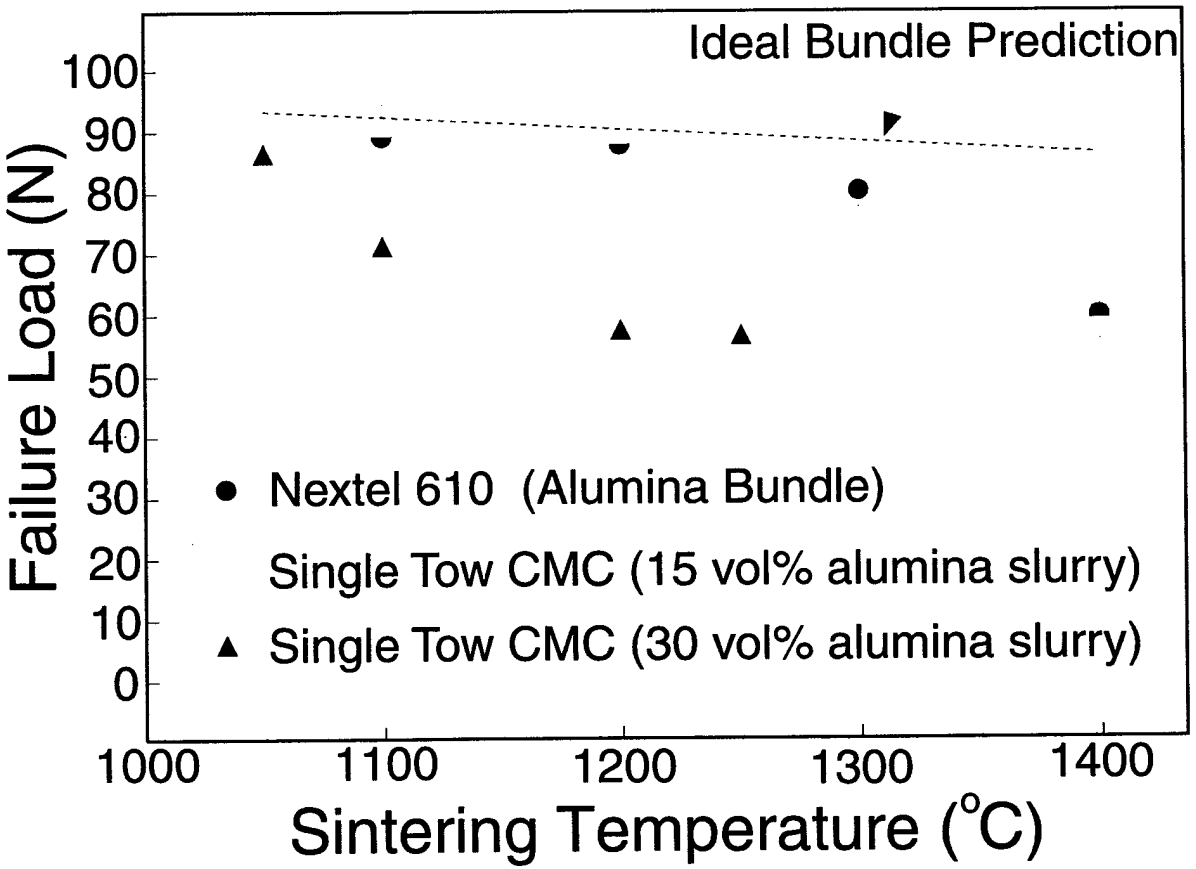
Ideal Bundle Prediction
Failure Load (N)
100
90
80
70
60
50
40
30
20
10
0
1000
1100
1200
1300
1400
Sintering Temperature (°C)
Nextel 610 (Alumina Bundle)
Single Tow CMC (15 vol% alumina slurry)
Single Tow CMC (30 vol% alumina slurry)

Conclusions

- Effects of Sintering on Alumina Single Filaments:
  - Strength Decreased.
  - Weld-line defects dominated at the highest sintering temperatures.
  - Grain size increased from 63 nm to 98 nm.

Conclusions

- Effects of Sintering on Alumina Bundles
  - The Ideal bundle model **predicted** the mechanical response of the as-received and low temperature (1300 °C) sintered alumina bundles.
  - The Ideal bundle model **overpredicted** the response of the high temperature (1400 and 1450 °C) sintered alumina bundles.
    - Filaments bonded together were no longer independent.
    - Fractography indicated filaments may fail at a lower stress when bonded together compared to being pulled apart.

Conclusions

- The Effect of Sintering on Alumina CMCs
  - At low interfacial shear strength, failure loads decreased with temperature due to filament/filament bonding
  - At high interfacial shear strength, failure loads probably decreased due to local load sharing.

THE CREEP BEHAVIOR OF AL_2O_3-BASED TOW AND HYBRID FIBERS

Vincent H. Hammond, Frank E. Wawner, and Dana M. Elzey

Background

The design of continuous fiber-reinforced composite systems for high temperature structural applications requires a complete understanding of the thermal and mechanical behavior of the constituents - i.e., the matrix and fiber. For many applications, such as power generation and aerospace systems, the most critical property is the ability of a material to resist time-dependent (creep) deformation at elevated temperatures.

The creep resistance and behavior of many candidate metal matrices currently under consideration for elevated temperature applications are well characterized. While some research has studied the creep of monolithic fibers and fiber bundles (1-4), the creep response of bundles is not well understood. In addition, although theoretical models have been proposed (5-8), no careful experimental studies have been used to verify or improve these models.

In this summary, the experimental results of creep tests performed on both alumina (Nextel 610) tows and alumina-porous alumina (A-PA) fibers will be presented and discussed. Also, the framework of a theoretical model currently being developed for predicting the fiber bundle creep response will be outlined.

Experimental

The A-PA fiber is prepared by pulling a Nextel 610 tow through an alumina slurry. The fiber is shaped and the organic binder is burned off, resulting in a "green" fiber. The A-PA is then sintered at elevated temperature to achieve the desired properties. More detail concerning the processing of the A-PA fiber can be found in an earlier section of this report (9). The final diameter of the A-PA fiber is approximately 300 μm.

Prior to testing, the sizing on the as-received Nextel 610 tows is burned off and replaced with a polymer coating to prevent damage during handling. The A-PA hybrid fiber is coated with a similar polymer coating. This coating is burned off the gage section during heat-up to the test temperature.

Creep tests were conducted using the apparatus shown in Figure 1. The system consists of an induction heater surrounding a nickel susceptor, a strain transducer (LVDT), load train, and sample grips. After the fiber is heated to the desired test temperature, a constant known load is applied. The LVDT outputs a voltage proportional to the elongation as a function of time, which is then recorded for analysis after the test is complete. All tests were conducted in air.

The fiber is removed from the heater after failure and saved for later study. In the case of the plain bundle tests, individual filaments are removed from the bundle, cleaned in acetone, and mounted on a sample holder for examination in a scanning electron microscope (SEM).

Similarly, the failure ends of the hybrid fibers are carefully removed and mounted for examination in the SEM.

It must be pointed out that the strains presented in this summary are based on a gage length of 2.375 inches, which is the physical height of the nickel susceptor. This is not an accurate indication of the gage length due to the presence of a temperature gradient within the susceptor (Figure 2).

Presently, there are two alternatives being considered. The first is known as the "effective gage length" proposed by Pysher (11). In this method, the temperature is measured as a function of position. The filament creep rate is determined using the equation generated by Wilson (10). The area of the creep rate / position curve is calculated. The temperature corresponding to the maximum creep rate is determined. This represents the height of a rectangle whose area is equal to the area under the creep rate / position curve. The gage length is then determined by calculating the length necessary to achieve this area. Using this new gage length, a new set of strain data is generated, which results in a new creep rate / position curve. This process is repeated until good agreement is reached (usually 3 iterations). This method results in a gage length of 1.73 inches.

The second method involves setting a minimum creep rate (temperature) below which elongation is negligible compared to that occurring in the hot zone of the furnace. A curve is then fit to the temperature profile, so that the temperature gradient may be modeled directly. A minimum temperature of 800 °C was selected as the lowest temperature of interest. Using this approach, a gage length of 3.25 inches was determined. A plot showing the influence of gage length on the strain is shown in Figure 3.

Results and Discussion

Alumina (Nextel 610) Tows

The creep response of single Nextel 610 (alumina) filaments has been well-characterized (10). The tests reported here have been performed primarily at 1000 and 1100 °C; but two tests were performed at 1200 °C.

Creep strain vs. time curves for three tests at 1100 °C are shown in Figure 4. From this figure, it can be seen that the creep response is predominantly steady state with little primary creep. A sharp increase of strain with time near the end of the tests (tertiary creep) signals imminent failure. Tertiary creep is not observed in tests on single Nextel 610 filaments (10), but has been found in tests of other tow fibers, including FP and PRD-166 bundles (3). The presence of tertiary creep in bundles is attributed to an increase in the effective applied stress due to progressive failure of individual filaments within the tow.

A comparison of creep rates for single Nextel 610 filaments and bundles is shown in Figure 5. Single filament data supplied by Dave Wilson of 3M (12) are shown using filled symbols, while the strain rates calculated from bundle tests are shown using open symbols. The stress exponents

(slope of the stress-strain curve) measured for single filaments and tow fibers are similar (Table1).

Fiber	1000 °C	1100 °C	1200 °C
Single filament	2.76	3.09	2.98
Tow fiber	4.11	2.94	2.38

Table 1: Stress exponents for Nextel 610 single filament and tow fibers.

By writing the steady state creep rate equation in the form

$$\varepsilon_{ss} = A\exp\left(\frac{-Q}{RT}\right)$$

The creep activation energy (Q) can be determined by plotting the natural log of the creep rate as a function of inverse temperature (T). Performing a series of tests using the same applied stress at different temperatures generates data for this analysis. Results of these tests are shown in Figure 6. By taking the slope of the linear regression fit to the data, the creep activation energy of the tow fiber was calculated as 630 kJoules/mole. This value is in good agreement with the activation energy of 660 kJoules/mole reported for the Nextel 610 single filaments (10). The good agreement in these creep parameters suggests that the bundle behaves primarily as a collection of filaments, with little interaction between individual filaments during creep.

Alumina – Porous Alumina (A-PA) Hybrid Fiber

Two sets of hybrid fibers were prepared for creep testing, one subjected to in-line sintering (ILS) at 1100 °C, the other sintered at 1400 °C. This was done to determine the influence of the sintering temperature on the creep response of the hybrid fiber. The normal sintering temperature of the hybrid fiber is 1100 °C. The second temperature was chosen because earlier tensile testing had shown that the strength of the hybrid fiber begins to decline when sintered at 1400 °C or higher. To date, all creep tests have been performed at 1100 °C.

Figure 7 compares the creep response of the Nextel 610 bundle and A-PA fiber (sintered at 1100 °C) at 1100 °C with an applied load of 3.5 pounds. It can be seen that the initial strain rates for the bundle and hybrid fiber are approximately the same. However, the failure strain and the time to failure of the hybrid fiber are roughly twice that of the bundle.

In Figure 8 is a similar plot for the A-PA fiber sintered at 1400 °C in which a dramatic reduction in creep rate is observed for the A-PA fiber. The differences in the creep response of these materials are detailed in the following table.

Fiber	ε_f	T_f (seconds)	ε_{ss} x 10^{-6} s^{-1}
Plain Tow	0.0595	1022	39.38
A-PA 1100 °C ILS	0.1168	2435	39.84
A-PA 1400 °C ILS	0.0789	26613	1.867

Table 2: Comparison of creep response of Nextel 610 bundles and A-PA fibers (T= 1100 °C, P=3.5 lbs).

A plot of creep rate versus stress for each of the three sample types tested at 1100 °C is shown in Figure 9. The dramatic reduction in creep rate (greater than an order of magnitude) for the 1400 °C sintered A-PA fiber relative to the bundle and 1100 °C sintered A-PA fiber is clearly shown. A comparison of the failure strains as a function of applied stress for all tests conducted at 1100 °C is shown in Figure 10. The failure strain of the A-PA fiber sintered at 1100 °C is the largest followed by the 1400 °C sintered A-PA fiber, and then the Nextel 610 bundle with the lowest strain to failure.

Figure 11 illustrates the time to failure as a function of stress for each of the three fibers. The low creep rate of the 1400 °C hybrid fiber coupled with a high strain to failure results in the long creep life. The low time to failure of the Nextel 610 bundle relative to the A-PA hybrid fibers is a consequence of its relatively high creep rate and low failure strain.

The results presented above indicate clearly that the addition of a porous alumina binder strongly alters the creep response of the conventional tow fibers. The reduction in creep rate and simultaneous increase in failure strain of the hybrid fiber relative to the plain bundle might be the result of load transfer between the filaments and the porous ceramic binder. This would explain the observation that a higher sintering temperature results in enhanced creep resistance since this would lead to a stronger bond between filaments and the binder, as well as between individual filaments, thereby resulting in improved load transfer. A consequence of the binder's ability to transfer load is that failed filaments may be reloaded at some point away from the initial failure.

The doubling of the failure strain of the 1100 °C fiber relative to the untreated bundle must be explained differently. The similar values of the creep rate for these two materials appear to rule out any large degree of load transfer between the filaments and binder.

Future work will focus on characterizing the failure surfaces of failed A-PA fibers. Samples from interrupted creep tests will be examined in an effort to determine the mechanisms responsible for the observed behavior. In addition, creep tests will continue on the current set of hybrid fibers at different temperatures to fully characterize their elevated temperature behavior. Hybrid fibers with a greater amount of porous binder will be tested to further investigate the influence of binder content on creep response. The understanding gained from these experiments will be used to optimize the microstructure and processing of the hybrid fiber for use in high temperature applications.

Modeling the creep behavior of bundles

Concurrent with the above experimental work, a theoretical model designed to predict the creep response of the Nextel 610 bundle is being developed. The model is micromechanics based in that it will use single filament properties to predict the bundle creep response. Thus, the creep response of the single Nextel 610 filaments (10) is used as input into the model. Therefore, it is hoped that any type of fiber bundle may be modeled by simply inputting the individual filament properties and bundle architecture.

The following assumptions are commonly made in the development of fiber bundle creep models (5-8):

1) No interaction between individual filaments.
2) Each fiber is of equal diameter and is equally loaded at t=0.
3) All creep elongation occurs in a gage length of uniform temperature.
4) Bundle exhibits global load sharing.
5) Failure of filaments obeys the weakest link theory (Weibull theory).

The initial development of the creep model used the above assumptions as a guide. However, there is a wide discrepancy between early model predictions and experimental results. Thus, it is necessary to re-evaluate the above assumptions.

In this experimental study, the existence of a temperature gradient within the heated susceptor precludes the assumption of a uniform temperature gage length. Additionally, the assumption of elastic behavior until failure is not valid. Therefore, the use of Weibull parameters based on elastic behavior at room temperature to model the elevated temperature creep response may not be an appropriate choice. Also, a more realistic bundle failure criterion based on experimental observations will be incorporated into the model. Once the model can successfully predict the response of the Nextel 610 bundle, a load transfer routine will be added to model the creep behavior of the A-PA hybrid fiber.

Conclusions:

The creep response of Nextel 610 bundles has been studied in the temperature range of 1000 - 1200 °C. Results indicate that bundles experience steady state creep until individual filaments begin failing within the bundle. Once failure initiates, the bundle enters a tertiary creep regime with failure imminent. Comparison of creep rate vs. stress plots for the bundle and single filaments show nearly identical behavior for all temperatures.

The study revealed that infiltration of the fiber bundle with an alumina slurry followed by sintering to produce a so-called "hybrid" fiber, results in a dramatically improved creep resistance. In particular, hybrid fibers sintered at 1400 °C exhibited creep strain rates more than one order of magnitude lower than for conventional (plain) bundles at the same applied load and temperature. In addition, hybrid fibers sintered at lower temperatures (1100 °C) display creep rates similar to plain bundles, but have approximately twice the strain to failure. Further experimental and metallographic studies, as well as model development, are being pursued in

order to understand the dependence of hybrid fiber creep behavior on processing and microstructural parameters.

References:

1) D. J.Pysher, N. Jia, R. J. Bodet, and R. E. Tressler, High Performance Composites for the 1990's, pp. 267-281, 1991.

2) R. E. Tressler and J. A. DiCarlo, High Temperature CMC (HT-CMC-1), pp. 33-49, 1993.

3) D. J. Pysher and R. E. Tressler, J. of Materials Science, Vol. 27, pp. 423-28, 1992.

4) G. Emig and R. Wirth, J. of Materials Science, Vol. 30, pp. 5813-18, 1995.

5) S. L. Phoenix, Advances in Applied Probability, Vol. 11, pp. 153-87, 1979.

6) M. Chrzanowski and J. Hult, Engineering Fracture Mechanics, Vol. 28, No. 5-6, pp. 681-688, 19987.

7) J. Neumeister, Engineering Fracture Mechanics, Vol. 35, No. 6, pp. 1081-92, 1990.

8) J. Bialkiewicz, Engineering Fracture Mechanics, Vol. 44, No. 5, pp. 711-20, 1993.

9) P. Cantonwine, Section B, this report.

10) D. M. Wilson, D. C. Lueneburg, and S. L. Leider, Ceramic Engineering and Science Proceedings, Vol. 14, No. 7-8, pp. 609-21, 1993.

11) D. J. Pysher, Ph. D. Dissertation, Dept. of Materials Science and Engineering, Penn State University, 1992.

12) D. Wilson, personal communication, 1998.

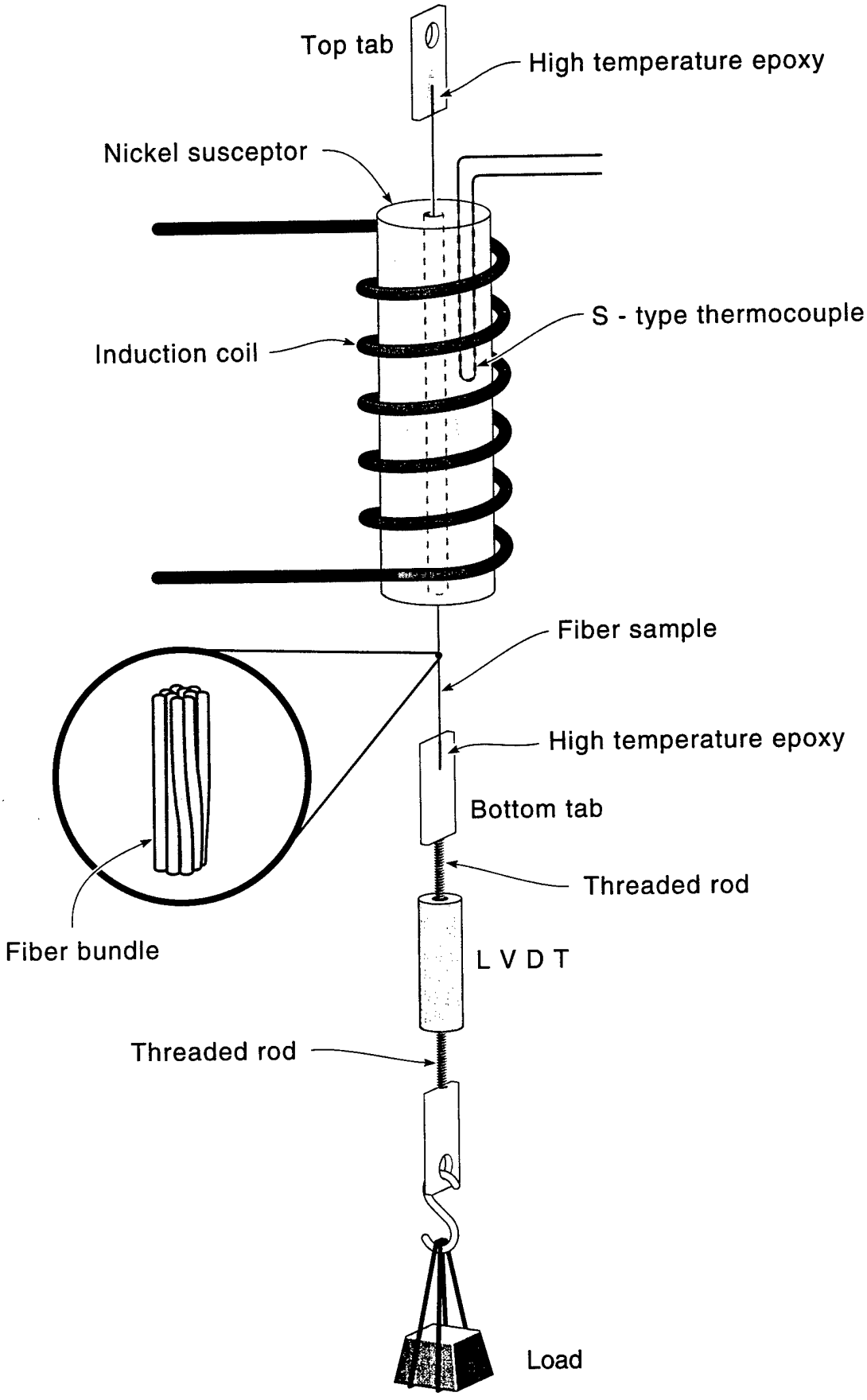

2440 nickel susceptor v hammond ipm 4/98

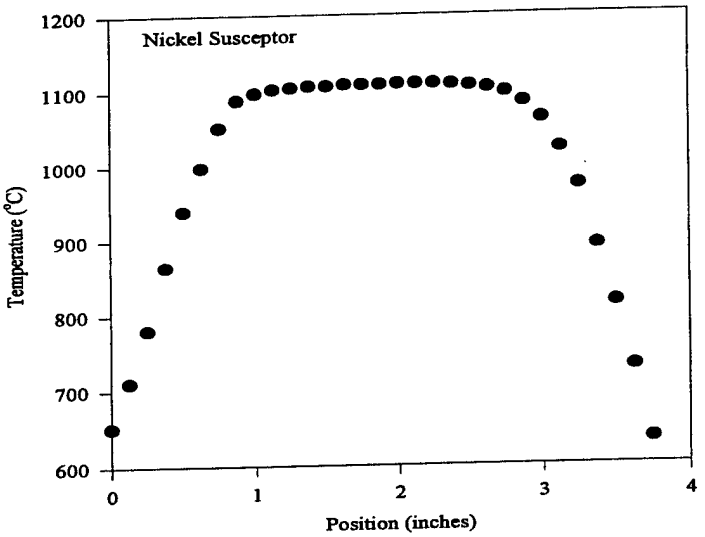

Figure 2: Temperature gradient at 1100 °C for the nickel susceptor.

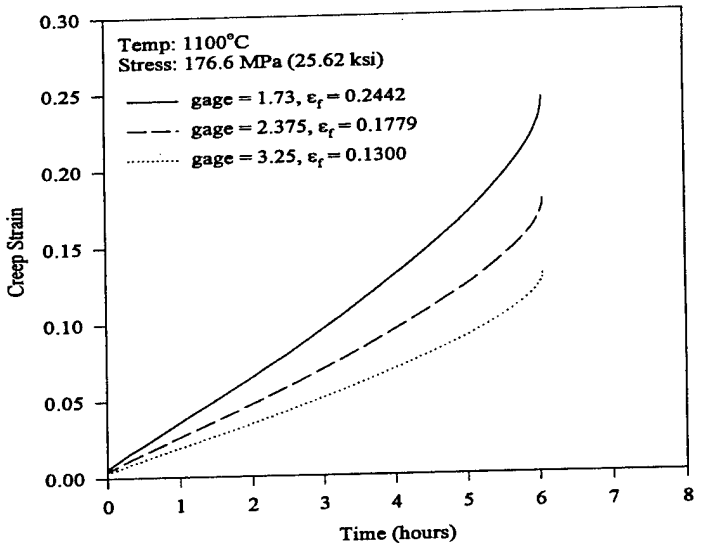

Figure 3: Effect of gage length on the calculated strain for a Nextel 610 bundle.

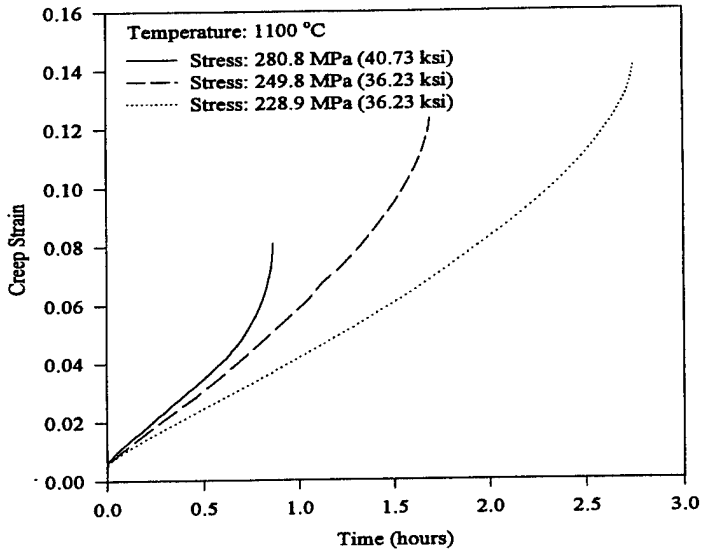

Figure 4: Representative creep curves for the Nextel 610 bundle at 1100 °C.

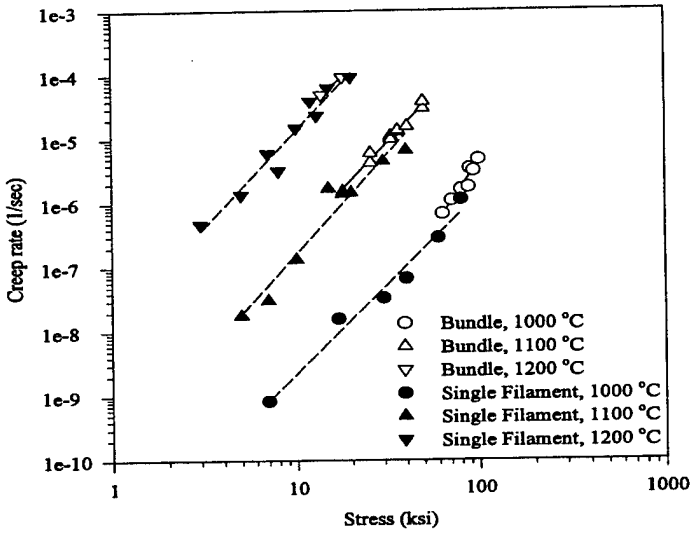

Figure 5: Comparison of the creep rates as a function of stress for single Nextel 610 filaments and Nextel 610 bundles for 1000, 1100, and 1200 °C.

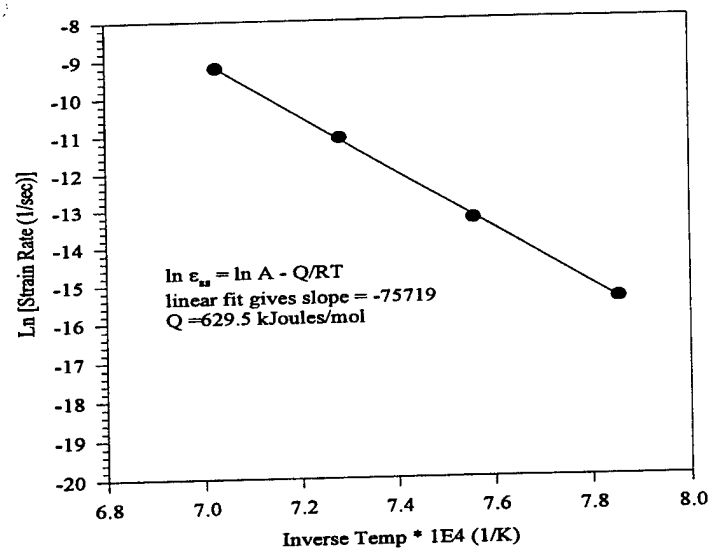

Figure 6: Calculation of creep activation energy for Nextel 610 bundle.

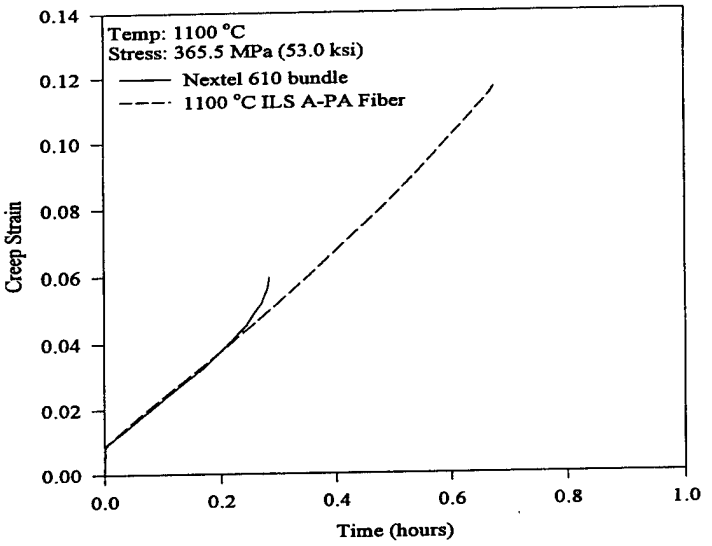

Figure 7: Creep curves for Nextel 610 bundle and 1100 °C sintered A-PA hybrid fiber.

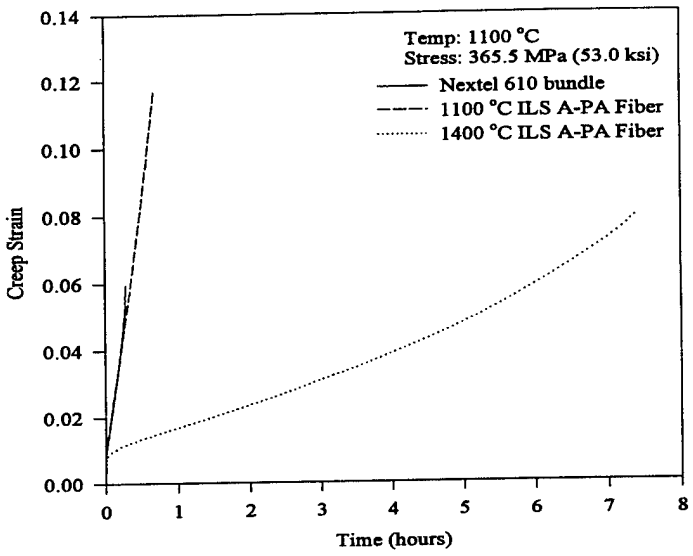

Figure 8: Creep curves for all three fibers tested at 1100 °C and $\sigma = 365.5$ MPa.

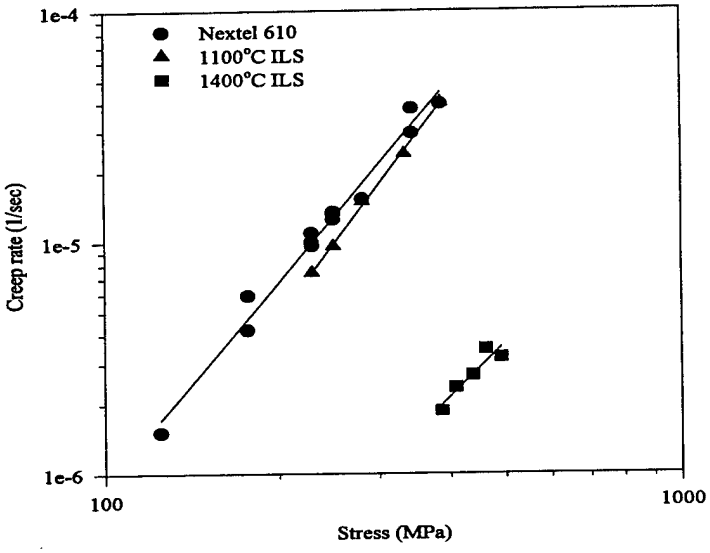

Figure 9: Creep rate as function of applied stress for the three fibers tested at 1100 °C.

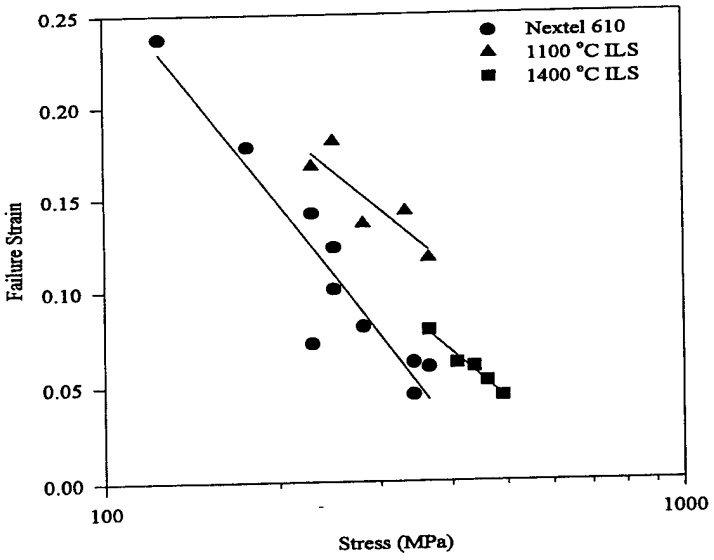

Figure 10: Failure strain as a function of applied stress for the three fibers tested at 1100 °C.

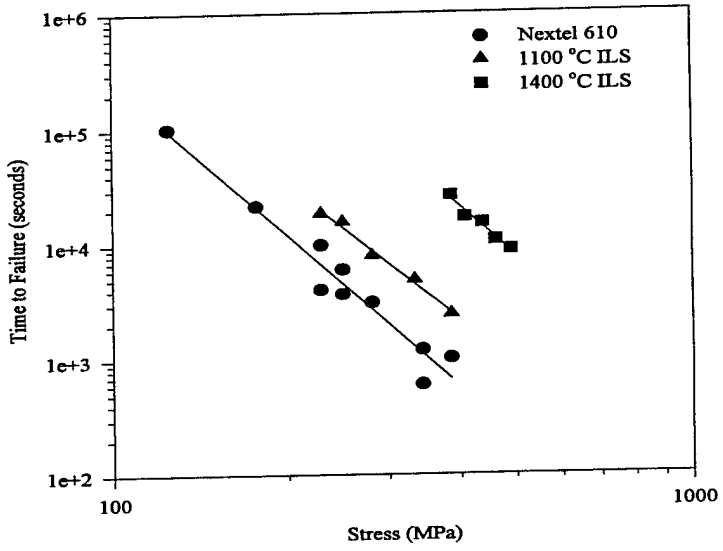

Figure 11: Time to failure as a function of applied stress for the three fibers tested at 1100 °C.

Creep Response of Nextel 610 Tows and A-PA Hybrid Fibers

V. H. Hammond, F. E. Wawner, and D. M. Elzey
Dept. of Materials Science and Engineering

Outline

- Background
- Experimental Set-up
- Test Results
  - Nextel 610 Bundle
  - A-PA Hybrid Fiber
- Modeling Approach
- Conclusions & Future Work

Background - Bundle Creep

- Experimental

  Pysher and Tressler: FP and PRD-166 (Al_2O_3)

  Emig and Wirth: Tyranno and Nicalon (SiC)

- Theoretical:

  Daniels: 1945

  Coleman: 1956 - 1958

  Phoenix, et al: 1978, 79

  Chrzanowski & Hult (1987), Neumeister (1990), Bialkiewicz (1993)

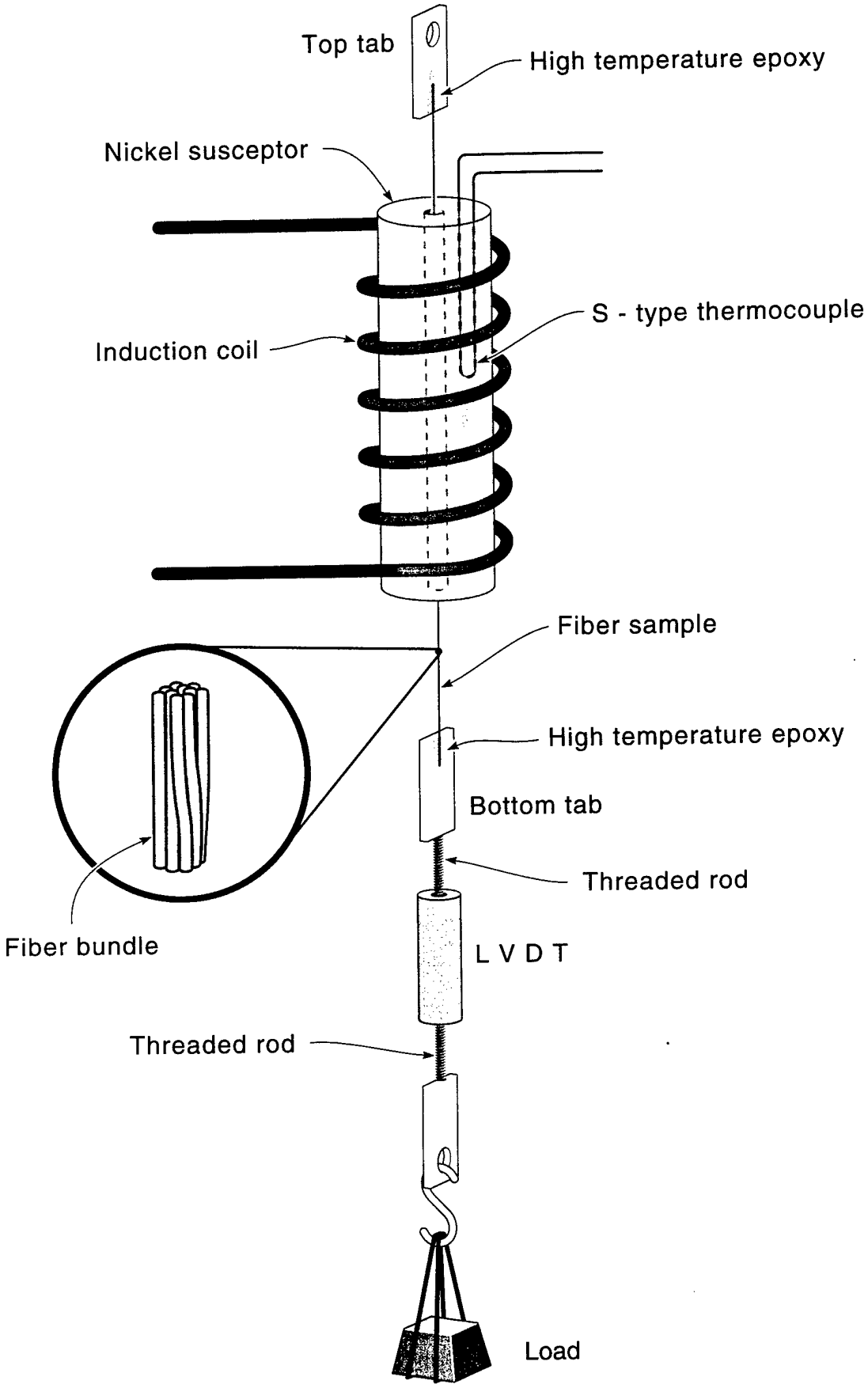

2440 nickel susceptor v hammond ipm 4/98

Gage Length Issues:

- Presently, use the actual height of the nickel susceptor as the gage length for determining strain. This is not correct as there is a temperature gradient along this length.

- Two options:
  1) Effective gage length: 1.73 inches
  2) Select minimum creep rate below which all strain is negligible. Use position dependent temperature profile to determine gage length. This results in 3.25 inches.

Gage Length Determination

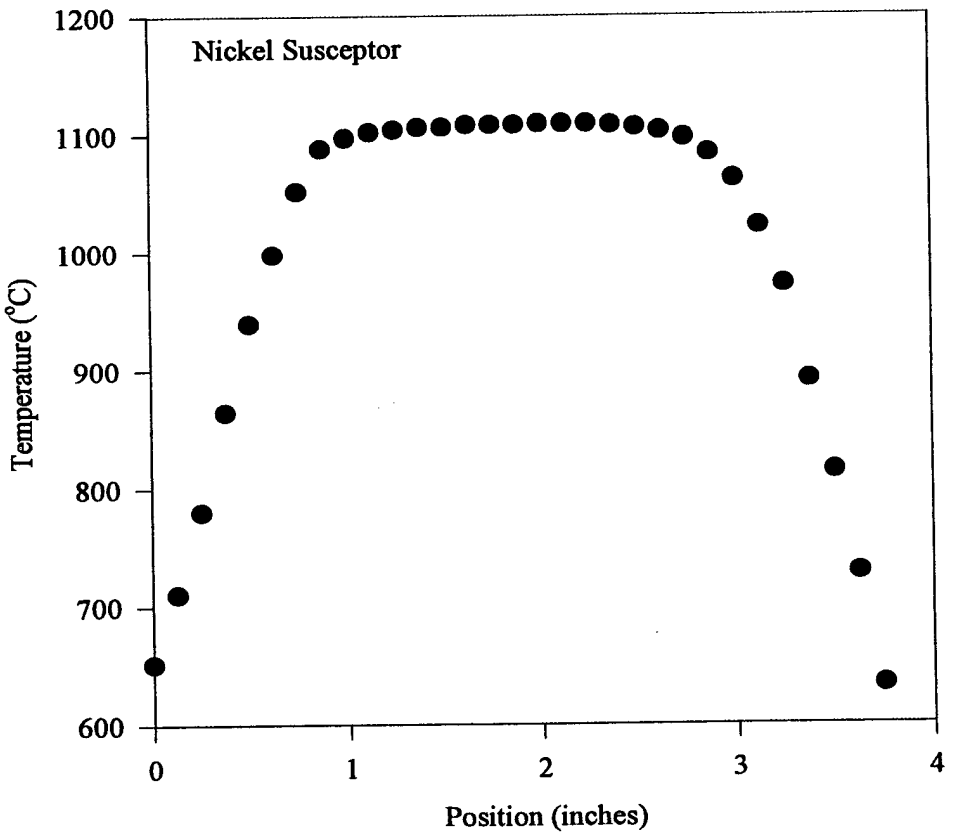

- Effective Gage Length: Determine area under curve. Calculate length required for equal area assuming isothermal temperature.

- Minimum Creep Rate: Determine minimum creep rate (or temperature) below which strain is negligible. Model the gradient profile over this length.

Actual Strain?

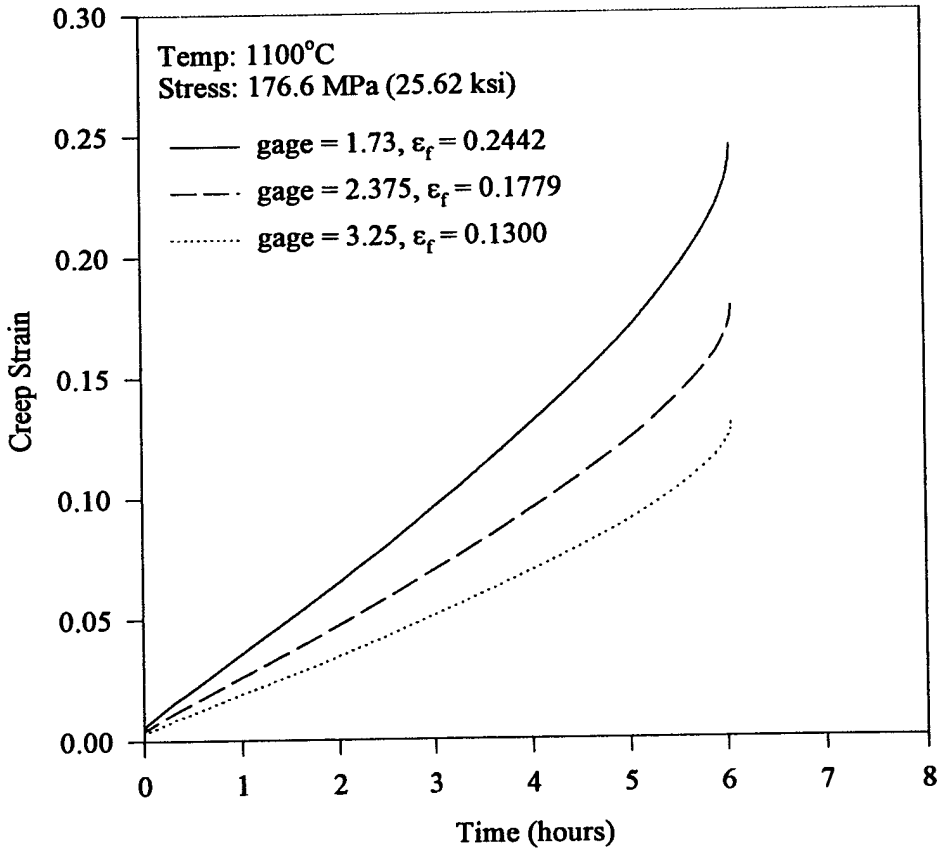

Representative Bundle Creep Curves

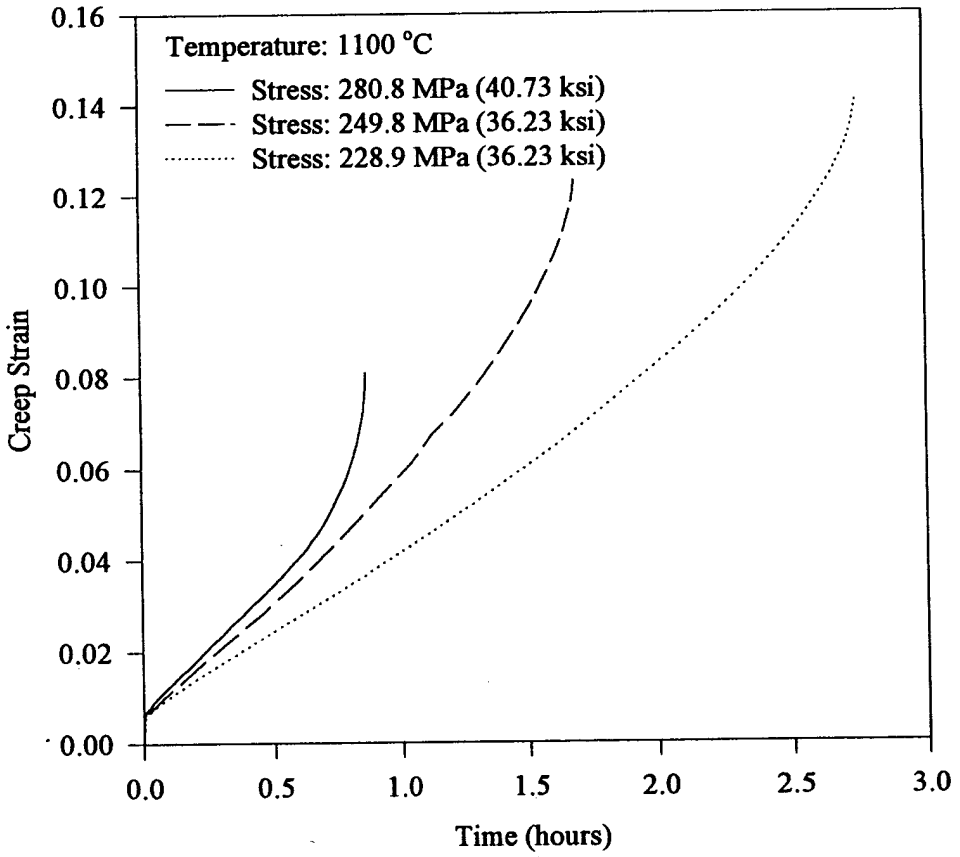

Creep Rate Comparison

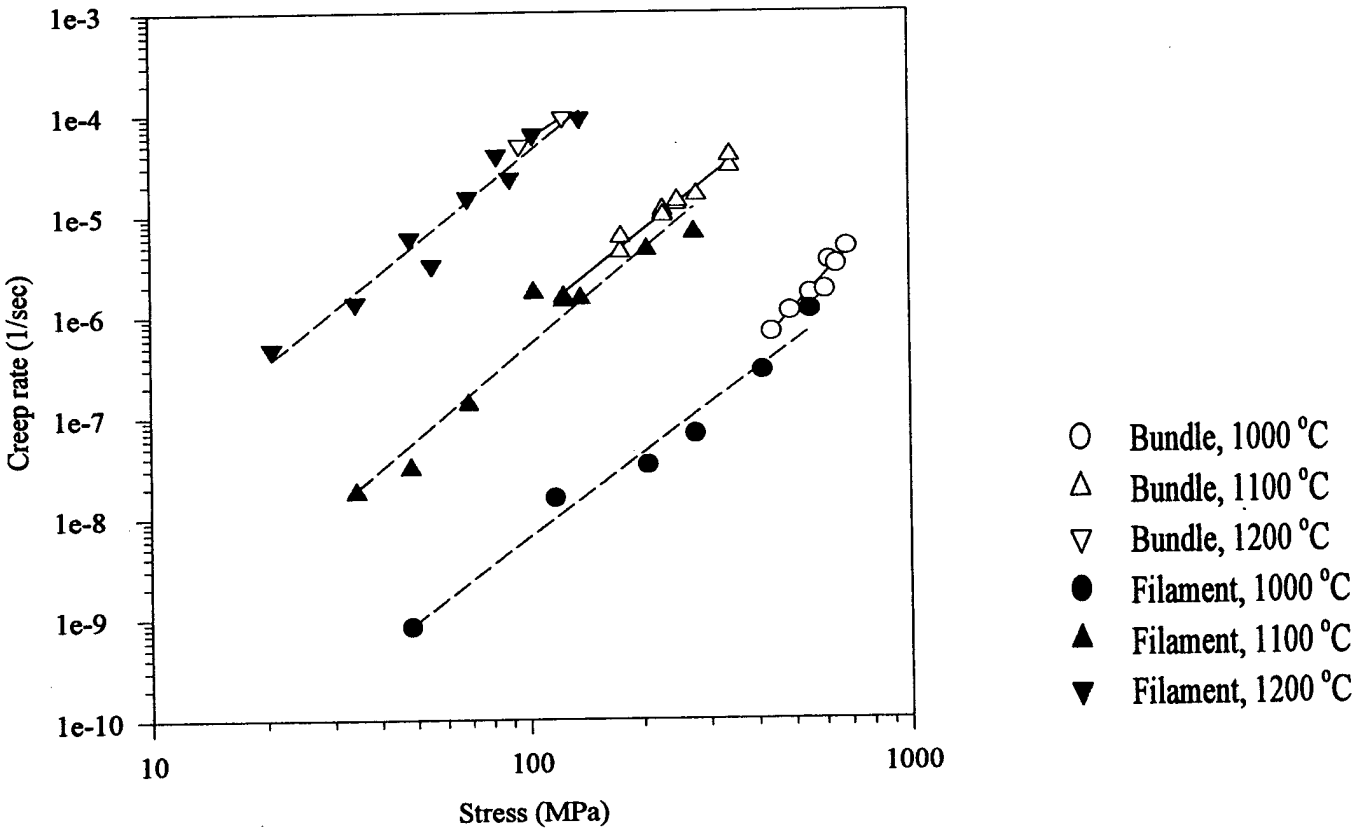

Filament Fracture Surface

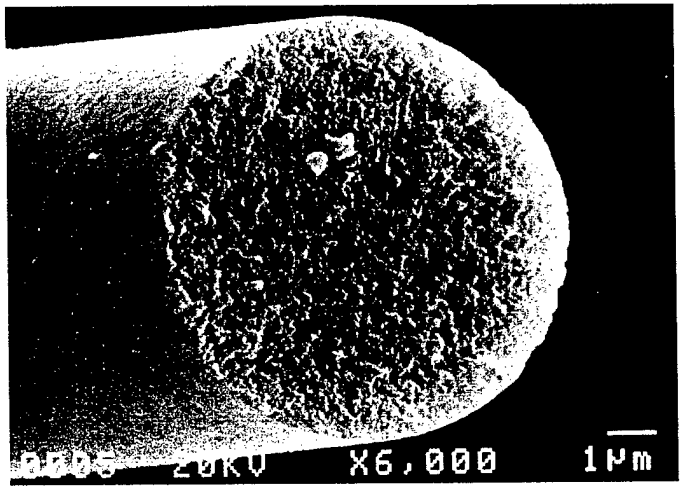

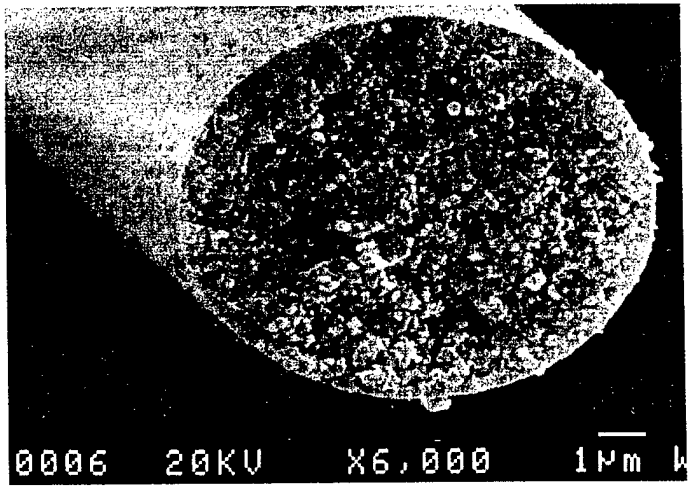

1100 °C
$\varepsilon_f = 0.1271$
$t_f = 8500$ s
$\sigma = 210$ MPa

1200 °C
$\varepsilon_f = >0.25$
$t_f = 4900$ s
$\sigma = 75$ MPa

A-PA Hybrid Fiber

- Two In-Line Sintering Temperatures:
  1100 °C and 1400 °C

- All hybrid fiber creep tests have been performed at 1100 °C.

A-PA Fiber Results - 1100 °C ILS

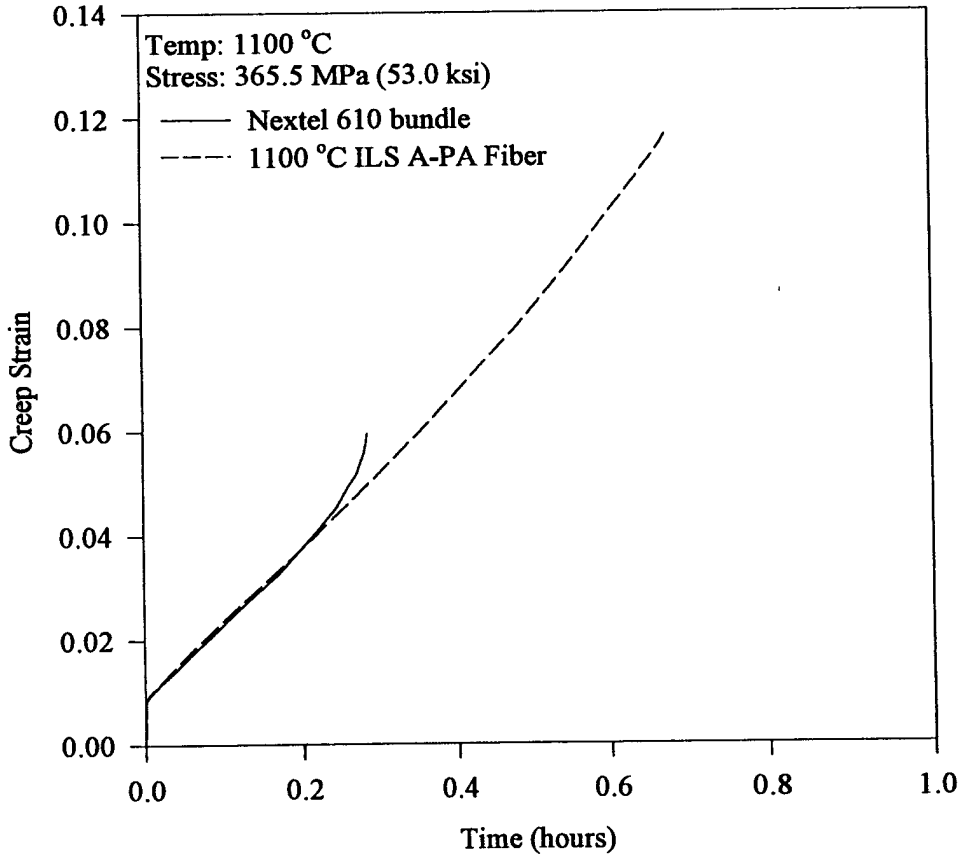

A-PA Hybrid Fiber - 1400 °C ILS

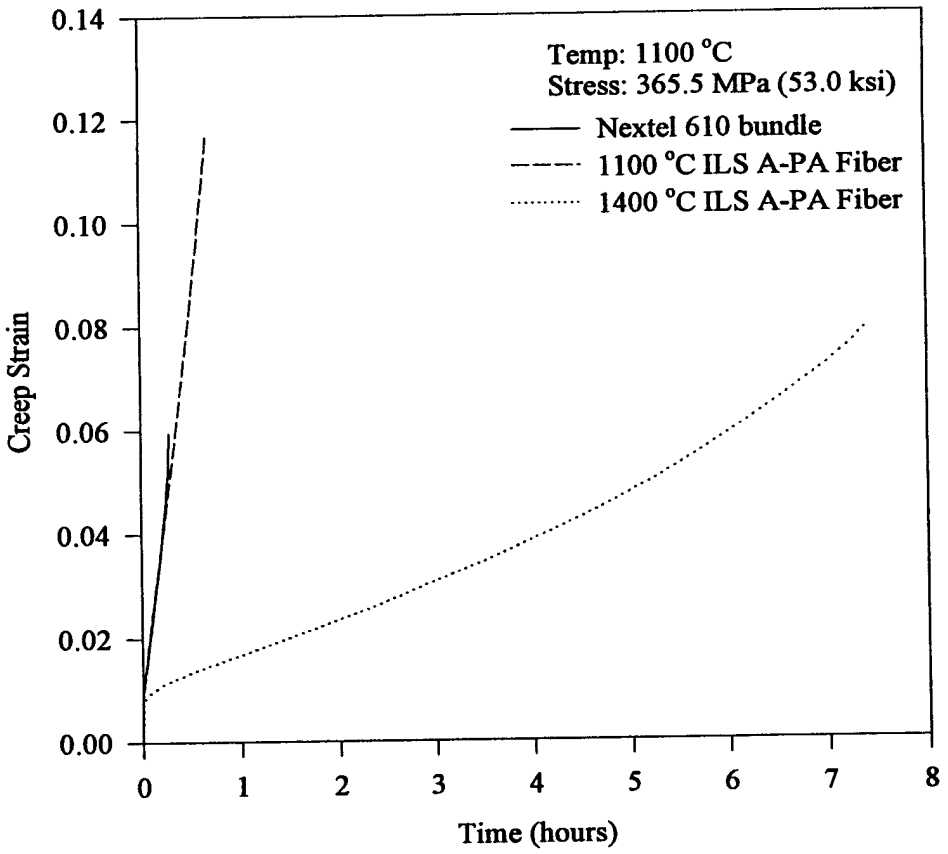

Comparison of Creep Response

Sample	ε_f	t_f (seconds)	ε_{ss} x 10^{-6} s^{-1}
Nextel 610	0.0595	1022	39.38
1100 °C ILS	0.1168	2435	39.84
1400 °C ILS	0.0789	26613	1.867

Creep Rate vs. Stress

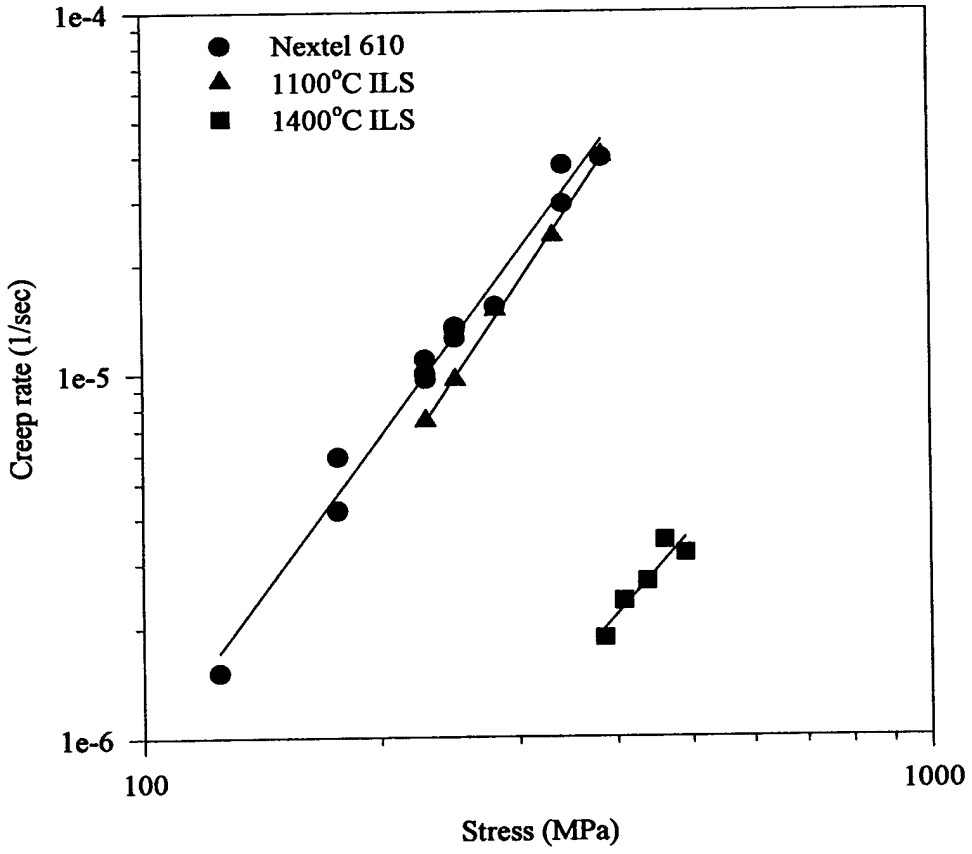

Failure Strain vs. Stress

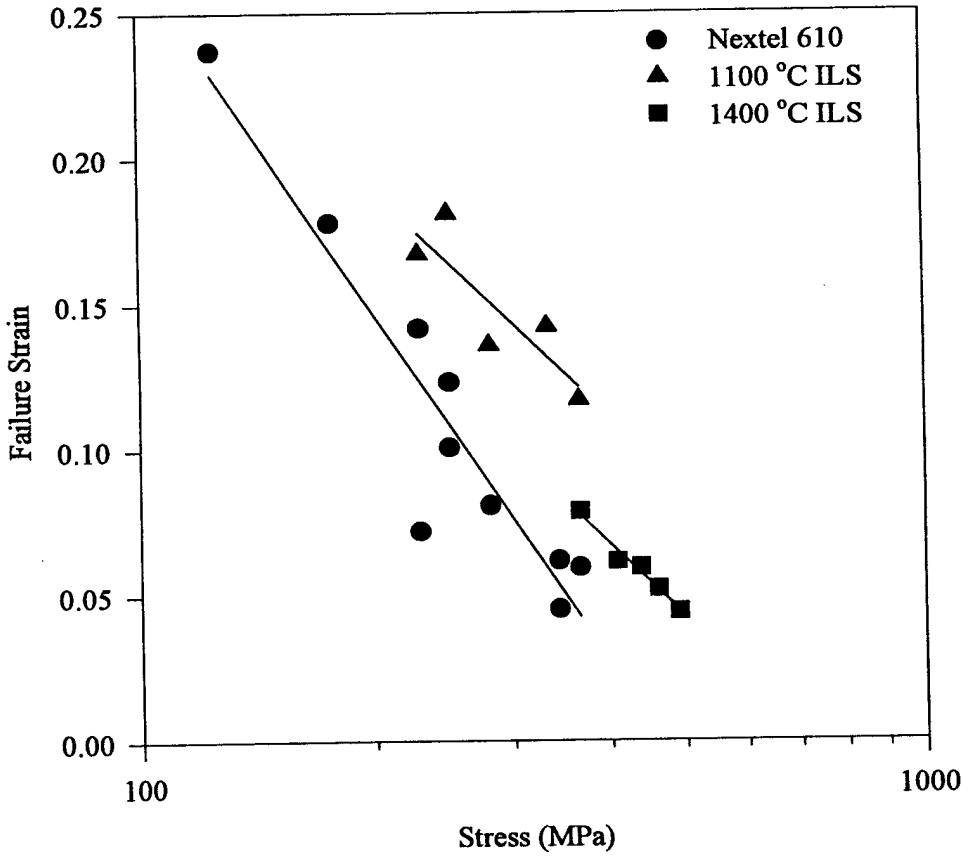

Time to Failure vs. Stress

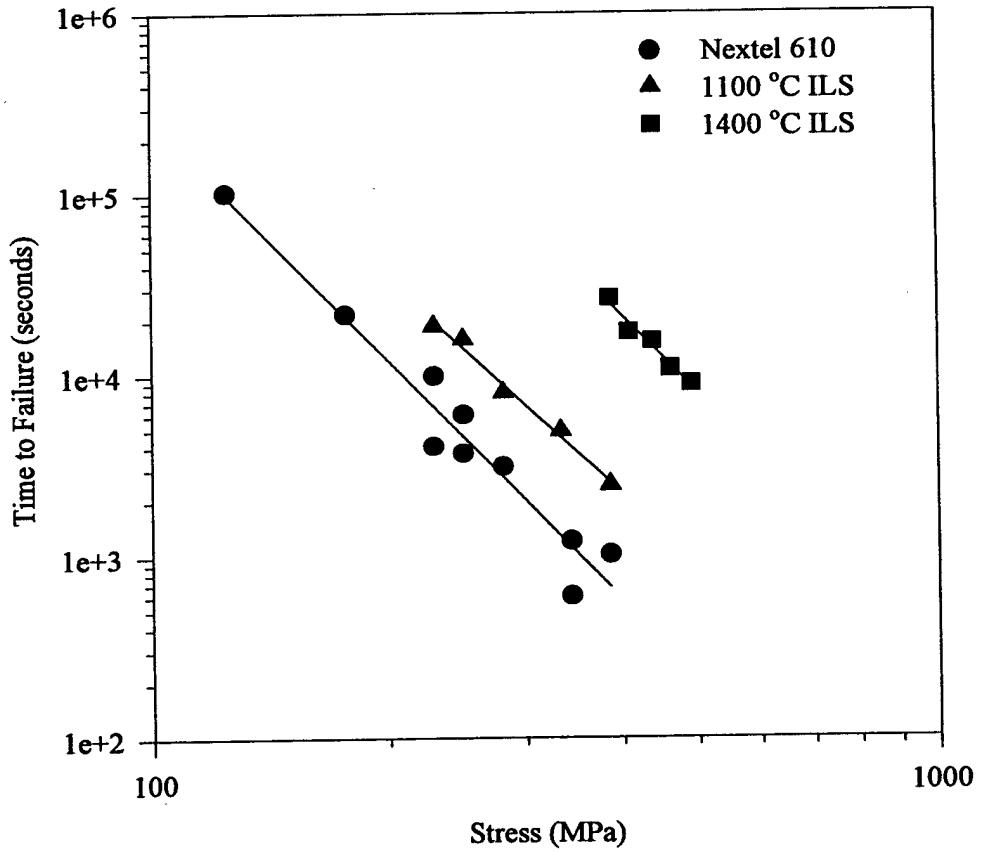

Modeling Approach

- Use single filament properties to model the creep response of the Nextel 610 tow.

- Assumptions:

  No interaction between individual filaments.

  Each fiber is equally loaded at t=0.

  Global load sharing.

  Failure of the filaments obeys the weakest link theory.

Conclusions

- The creep rates of Nextel 610 bundles and single filaments are in good agreement.
- Bundles show tertiary creep behavior.
- The addition of the porous binder dramatically alters creep response:

  1100 °C: similar creep rates. failure strain is roughly double.

  1400 °C: creep rate reduced by order of magnitude.

Future Work

- Characterize failure mechanisms.
- Continue creep testing:
  - evaluate current set of hybrid fibers at other temps.
  - perform tests on hybrid fibers with increased binder content.

- Continue model development.

PLASMA SPRAY PROCESSING OF NICKEL ALUMINIDE

Vincent H. Hammond, Frank E. Wawner, and Dana M. Elzey

Background:

The purpose of this grant was to develop a cost-effective composite which could be used at higher temperatures than currently possible with the silicon carbide/titanium matrix systems. Two problems currently hinder widespread usage of this system at elevated temperatures: 1) fiber/matrix reactivity, and 2) oxidation of both the matrix and fiber which results in a degradation of composite performance. Both of these problems were addressed by looking at a alumina fiber reinforced nickel aluminide. Nickel aluminides possess a higher oxidation resistance than the titanium systems (1), while alumina is thermodynamically stable in the nickel based matrix.

This phase of the project was centered on the use of plasma spray deposition to manufacture both neat and A-PA fiber-reinforced tapes of IC-50. IC-50 has a nominal composition of Ni - 23% Al - 0.5% Hf - 0.2% B (atomic %). The alloy was supplied by Praxair Specialty Powders with a size distribution of 44 - 120 μm and a mean size of approximately 80 μm. Hafnium is added for solid solution strengthening and to improve creep resistance. The addition of boron has been found to dramatically improve room temperature ductility by suppressing intergranular fracture.

In the plasma spray process, matrix powder is injected into a plasma torch. The high temperature of the plasma torch melts the particles, which are then directed onto a rotating substrate located directly beneath the torch. The molten droplets solidify on the substrate, resulting in tapes which can be stacked, oriented, and consolidated into the final neat matrix or composite part.

Deposition was conducted using a 100 kW RF induction coupled plasma spray system manufactured by Tekna Plasma Systems, Inc. The plasma is created by passing the gas mixture through a 5 turn induction coil centrally mounted above a vacuum chamber. Controls are used to monitor chamber pressure, gas flow, mandrel motion, powder feed rate, and power settings. After deposition, the foil was removed and inspected both visually and with the aid of a SEM. Phase identification was performed via x-ray diffraction. Selected samples were analyzed to determine the level of contaminants picked up during spraying.

Experimental Results:

Neat Foils

Initial deposition experiments used an argon/hydrogen (Ar/H_2) plasma. These foils were coated with a black "soot" - like residue. SEM examination revealed the presence of fine micron-sized particles on the surface of the foil (Figure 1a). It was thought that the particles were the result of contamination from the carbon mandrel used as the deposition substrate. However, replacement of the graphite mandrel with a 304 SS mandrel had no influence on the quality of the deposited

material. Altering the amount of hydrogen used in the plasma gas also had little effect on the foil quality.

One possible explanation for the presence of the residue is the high enthalpy of the Ar/H_2 plasma, which may have resulted in the formation of a IC-50 vapor cloud inside the chamber. Upon cooling, small particles may have condensed from the vapor and deposited on the foil surface and chamber walls. Similar vapor phase condensation has been observed in the induction plasma treatment of alumina powders (2).

A new set of experiments was conducted using an argon/helium (Ar/He) plasma. As the Ar/He plasma has a lower enthalpy, or heat content, than the Ar/H_2 plasma, it was hoped that the amount of the powder residue would be greatly reduced. Indeed, the deposited foils had a much cleaner surface appearance, and SEM examination showed a significant reduction in the number of micron-sized particles on the foil surface (Figure 1b).

Representative samples from both deposition experiments were analyzed using x-ray diffraction to determine the phase of the deposited material. Scans from both sets of foils were identical. A diffraction pattern for an Ar/He foil is shown in Figure 2, along with a reference pattern for Ni_3Al. Although there is a slight shift to higher 2θ values in the experimental pattern, the close correlation clearly identifies the deposited material as Ni_3Al. The slight shift has been attributed to either the non-stoichiometric nature of the deposited IC-50 or the presence of residual stresses in the foil (3).

An equally important criterion in determining foil quality is the amount of contaminants (i.e. - oxygen and hydrogen) present in the deposited foils. Samples were sent to Leco Corporation where the amount of oxygen and hydrogen present in each foil type were measured. The results from these tests are given in the following table.

Table 1: Oxygen and hydrogen content in as-received IC-50 powder and plasma-sprayed foils.

Sample Type	Oxygen, in wt. %	Hydrogen, in ppm
IC-50 powder	0.0133	3.1
Argon/Hydrogen foil	0.0631	52.1
Argon/Helium foil	0.0411	7.8

From this table, it is clear that the foils deposited with the Ar/H_2 plasma had a significantly higher amount of both oxygen and hydrogen. The hydrogen is thought to occupy interstitial sites in the lattice. An increase in the amount of interstitial hydrogen was observed in spray deposited Ti-6-4 and Ti-6-2-4-2 monotapes (4)

Fiber-Reinforced Tapes

Based on the above results, a standard procedure for spraying neat IC-50 was developed which resulted in good quality, reproducible foils. This same procedure was used when work began on spraying A-PA fiber reinforced tapes.

Prior to each run, the mandrel was cleaned to remove any residue from the previous run. Approximately 8 - 10 rows of A-PA fiber was wound onto the mandrel using a low-speed lathe. In this way, both fiber alignment and tension was constant for each experiment. A 1" steel plate was laid across the fibers to hold them in place during the deposition.

After the fibers were secured, the mandrel was positioned in the chamber and pre-heated for 10 minutes using the plasma. The fibers survived this aspect of the deposition procedure very well. However, once spraying began, some of the A-PA fibers developed hot spots, usually at kinks which tended to lift off the mandrel. The fibers eventually failed at these spots and fell off the mandrel. Approximately 50% of the fibers were lost in this manner, usually in a random manner. Attempts at altering spraying height, plasma composition, or powder feed rate made little difference in the failure of the fibers during spraying.

Despite the loss of several fibers, each spray run was completed. A visual inspection of the tape was conducted after the run was completed. There was a tendency for the deposit on top of the fibers to lift off, leaving the individual fibers exposed. In addition, there was only a small amount of material deposited between the fibers. These problems were thought to be interrelated, in that the deposit lift-off resulted from a lack of cohesion between the deposit on top of the fibers and the material deposited between the fibers. The poor filling between the fibers was attributed to the rough fiber surface, which prevented the molten droplets from flowing into the inter-fiber gaps before they solidified. For comparison, both SCS-2 and SCS-6 fibers were wrapped onto the mandrel and sprayed, using identical conditions as used during the A-PA spraying experiments. None of the above difficulties were experienced when spraying these fibers.

Conclusions:

The feasibility of using plasma spray deposition for producing neat foils of a nickel aluminide, namely IC-50, has been verified. Early attempts using an argon/hydrogen plasma torch resulted in poor quality foils with a high level of oxygen and hydrogen. In addition, a large amount of surface contamination in the form of micron-sized particles was noticed. The presence of the particles was attributed to vapor phase condensation resulting from the high enthalpy of the torch. When the plasma gas mixture was switched to argon/helium, the deposited foils had a better appearance and a lower level of contaminants. X-ray diffraction showed that, in both cases, the deposited material was Ni_3Al.

However, several problems were encountered when attempting to produce fiber reinforced tapes. The primary difficulty was that the A-PA fiber tended to break when the spraying process was started. Other problems included inadequate deposit between fibers and a tendency for the deposited alloy to lift off the fibers upon cool-down. The inability to overcome these difficulties

despite trying a number of approaches precludes the use of plasma spray deposition for manufacturing A-PA fiber-reinforced IC-50 tapes.

References:

1. C. M. Ward-Close, R. Minor, and P. J. Doorbar, Intermetallics, 4, 217 (1996).

2. T. Ishigaki, Y. Bando, Y. Moriyoshi, and M. I. Boulos, Journal of Materials Science, 28, 4223 (1993).

3. X. Liang and E. J. Lavernia, Scripta Metallurgica and Materialia, 29, 353 (1993).

4. H. Gigerenzer and A. J. Kumnick, Plasma Processing and Synthesis of Materials III, p. 29, Materials Research Society Symposium Proceedings, Vol. 190, Pittsburgh (1990).